Wavelet analysis of deep-tow magnetic profiles: Modeling the magnetic layer thickness over oceanic ridges

Gaud Pouliquen[1]
Laboratoire de Gravimétrie, Institut de Physique du Globe, Paris, France

Pascal Sailhac
Laboratoire de Proche Surface, EOST, Strasbourg Cedex, France

Received 24 August 2001; revised 22 May 2002; accepted 30 December 2002; published 13 June 2003.

[1] The interpretation of marine magnetic anomalies usually consists either in determining the magnetization distribution assuming the source geometry and magnetization direction or in determining the magnetic layer thickness assuming the magnetization direction and intensity. In this paper, we introduce a new technique that allows modeling of the thickness of the magnetic source layer with very few a priori assumptions about the magnetization: the magnetic layer is assumed to be made of a series of bodies, each having a constant unknown magnetization and an unknown size. This technique is based upon the application of the continuous wavelet transform recently introduced for the interpretation of potential field data as a multipole decomposition. We present applications to synthetic data, to one deep-tow magnetic profile recorded across the Juan de Fuca Ridge (JDF), and to three deep-tow magnetic profiles recorded across the Central Indian Ridge (CIR). Our results confirm that despite significant source thickness variations (100–1200 m across the CIR), measured magnetic anomalies mostly reflect past geomagnetic field intensity fluctuations; however, we show that within the axial region of high magnetization, thickness variations have a significant contribution to short-wavelength variations of deep-tow magnetic signals (>100 nT). *INDEX TERMS:* 0903 Exploration Geophysics: Computational methods, potential fields; 0930 Exploration Geophysics: Oceanic structures; 1517 Geomagnetism and Paleomagnetism: Magnetic anomaly modeling; 3005 Marine Geology and Geophysics: Geomagnetism (1550); 3035 Marine Geology and Geophysics: Midocean ridge processes; *KEYWORDS:* wavelet transform, multipole decomposition, magnetic anomalies, source layer thickness, mid-ocean ridges

Citation: Pouliquen, G., and P. Sailhac, Wavelet analysis of deep-tow magnetic profiles: Modeling the magnetic layer thickness over oceanic ridges, *J. Geophys. Res.*, *108*(B6), 2297, doi:10.1029/2001JB001459, 2003.

1. Introduction

[2] Marine magnetic anomalies are attributed to horizontal variations of magnetization intensity in the magnetic source layer which is usually considered to be the highly magnetized extrusive basalts layer [*Talwani et al.*, 1971; *Tivey*, 1996]. These magnetization contrasts are controlled by several factors, whose contribution is debated: variations of the magnetic layer thickness, variations in magnetic properties of the source material, fluctuations of the geomagnetic field intensity, direction, and polarity reversals. The magnetic layer thickness over oceanic spreading centers is poorly constrained and previous studies were limited to fast spreading ridges and young oceanic crust [*Lee et al.*, 1996]. Hence most studies of marine magnetic data concern the intensity of the remanent magnetization and neglect source thickness variations. Some authors have nonetheless proposed that source thickness variations can contribute to short-wavelength magnetic anomalies [*Tivey and Johnson*, 1993].

[3] During a recent cruise over the Central Indian Ridge (CIR), three deep-tow magnetic profiles have been acquired, extending symmetrically from the axis out to 3.5 Ma crust. The first interpretation of these data [*Pouliquen et al.*, 2001] was based on classical processing and inversion techniques in the Fourier domain (method of *Parker and Huestis* [1974]). It was concluded that the magnetic anomalies along the profiles reflect primarily the intensity fluctuations of the geomagnetic field during the past 3.5 Myr. The validity of this interpretation was limited by the assumption that the magnetic layer has a constant thickness along the profiles.

[4] A number of inversion techniques have been used to evaluate source layer thickness from surface, airborne and deep-tow marine magnetic profiles [*Macdonald*, 1977; *Hansen and Simmonds*, 1993; *Tivey and Johnson*, 1993; *Lee et al.*, 1996; *Schouten et al.*, 1999]. All of these techniques require a priori information on the source intensity and

[1]Now at Total, E&P, Potential Field Methods, Paris, France.

0148-0227/03/2001JB001459$09.00

direction. Powerful techniques such as analytic signals [*Nabighian*, 1972, 1974], Euler deconvolution [*Thompson*, 1982] and Werner deconvolution [*Hansen and Simmonds*, 1993] have been developed to perform an automatic characterization of potential field sources along profiles; they apply quite well for the horizontal source positions but not for their depth because of noise limitations.

[5] Recently, *Moreau et al.* [1999] have shown that the analysis of potential fields with a continuous wavelet transform avoids a number of drawbacks of these earlier methods. Basically, one can use the continuous wavelet transform as an analyzing tool of potential field data to enhance the local wavelength information of each source, reduce the noise and provide a simple inverse scheme. This allows for the determination of source parameters such as the horizontal position and depth of the source, and a shape index similar to the structural index used in Euler deconvolution. *Sailhac et al.* [2000] have shown how to use complex wavelets to interpret magnetic data without using either the azimuth of profiles or the inclination of magnetization to characterize local and extended magnetic sources such as vertical and inclined steps and strips. They proposed an automated method for the estimation of source thickness, which was then adapted and applied to gravity data [*Martelet et al.*, 2001].

[6] Now we propose a method that uses wavelet transform of deep-tow magnetic profiles to characterize the magnetization contrasts of the magnetic source layer; this provides estimates for their horizontal location, height, and intensity. We first show that this method is adapted to handle marine magnetic anomaly profiles; we test its application to synthetics and to one observed deep-tow magnetic profile in a well-known region of the Juan de Fuca Ridge (JDF). Then we apply it to the three CIR deep-tow magnetic profiles. We use the results to test our previous interpretation that short-wavelength magnetic anomalies recorded along these profiles primarily reflect field intensity variations [*Pouliquen et al.*, 2001]. We eventually discuss temporal variations of the thickness of the magnetic source formed at this intermediate spreading ridge.

2. Magnetic Source Thickness at Mid-Ocean Ridges

[7] In this section, we first review classical and recent methods used to interpret magnetic signal at mid-ocean ridges, and then we give an overview of what is known of the magnetization structure of the oceanic crust.

2.1. Magnetic Signal and Source Characteristics

[8] We consider a two-dimensional distribution of magnetization $J(x)$ (x being the across-axis direction) which is confined between an upper surface $z_1(x)$ and a lower surface $z_2(x)$. While both z_1 and z_2 are constant, the resulting total field magnetic anomaly $\delta T(x)$ measured along the x axis above the upper surface is expressed by a well-known convolution integral [*Bott*, 1967; *Blakely*, 1996]:

$$\delta T(x) = \int_{-\infty}^{+\infty} J(\xi)\mathrm{K}[z_1, z_2, \theta, (x-\xi)]d\xi, \qquad (1)$$

where θ is a function dependent of the magnetization direction. This convolution equation shows that the anomaly δT is fully described by two independent functions J and K. While the kernel function K depends on many attributes of the layer (its depth and thickness and the directions of the magnetization and of the main field), the source magnetization distribution function J is a function of x only. In the case of across-axis profiles at mid-ocean ridges, J is therefore a function of time ($t = x/u$, with u being the half spreading rate). J reflects either variations of the magnetic properties of the magnetic carriers (such as the natural remanent magnetization (NRM) decrease of basalts due to low-temperature alteration [*Bleil and Petersen*, 1983]) or geomagnetic field variations (intensity fluctuations and polarity reversals). Usually, the direction of magnetization is assumed to be parallel to the direction of the regional magnetic field whereas changes in the direction of magnetization (e.g., due to tectonics [*Courtillot et al.*, 1980; *Verosub and Moores*, 1981]) are neglected, so that θ is known. Hence determining source parameters can focus on the magnetization distribution J and on the depth and thickness of the source (i.e., z_1 and z_2). Convolution equation (1) shows that the magnetization distribution J is linearly related to the amplitude of magnetic anomalies, but that the behavior of the filter K with the source depth and thickness is not linear. Equation (1) is still valid when only one or both of the two variables z_1 and z_2 varies along the x axis. However, in that case, equation (1) is not a convolution and inversion cannot be applied using a simple deconvolution algorithm. It is necessary in that case to consider more complex algorithms, e.g., a series of local deconvolutions like the Werner deconvolution technique [*Hansen and Simmonds*, 1993].

[9] In practice, it is therefore easier to invert the observed signal for J, assuming constant values for both the depth and thickness of the magnetic source layer, than to perform an inversion for these two other source parameters. Indeed, over relatively long periods (i.e., $\sim$500 kyr or more), marine magnetic anomalies probably do reflect mostly intensity and/or polarity variations of the geomagnetic field. At those timescales, source thickness variations caused by the complex geometry of the accretion process are probably smoothed [e.g., *Wittpenn et al.*, 1989]. This may not be the case over shorter time periods ($\sim$30–100 kyr), corresponding to the short-wavelength magnetic anomalies also known as "tiny wiggles." Some authors argue for a geomagnetic origin of these tiny wiggles [*Cande and Kent*, 1992], while others propose that they are caused by short-wavelength source thickness variations [*Klitgord et al.*, 1975; *Tivey and Johnson*, 1993]. At these short timescales, the interplay of various source parameters and the non unicity of solutions to the inverse problem must be taken into account. Let us consider for example the result of a simple deconvolution of the anomaly caused by a two-block model, each block having a different thickness and intensity (Figure 1). Using a kernel with constant 1-km thickness, the resulting magnetization model looks like a high-frequency version of the magnetic anomaly but differs from the initial magnetization model. This example illustrates the intrinsic limitation of a basic deconvolution-based technique which assumes a constant thickness for the source, whereas the inverse problem should consider both the thickness and the magnetization parameters

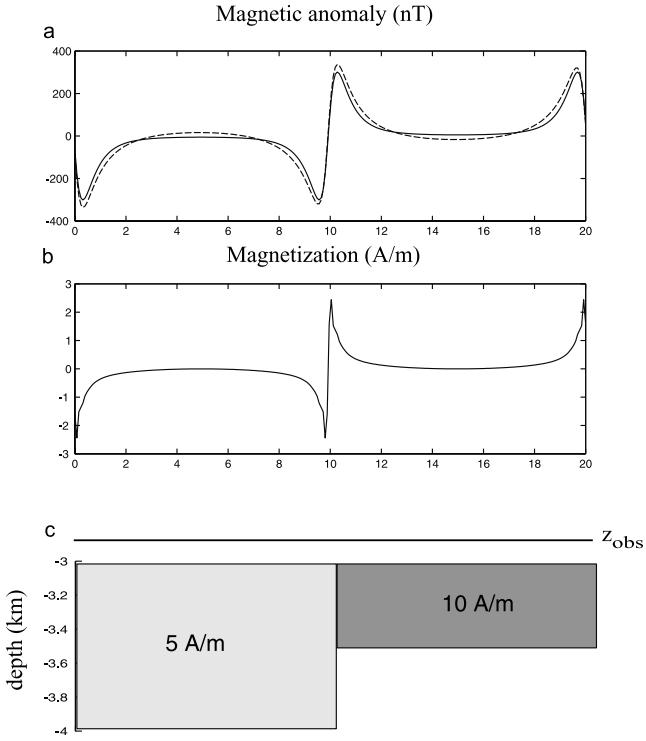

Figure 1. (a) Solid line shows the magnetic anomaly created by the source presented on Figure 1c. The anomaly was reduced to the pole. Dashed line shows the anomaly computed from the magnetization obtained by inversion (*Parker and Huestis* [1974] method) of the previous anomaly with a constant layer thickness of 1 km. (b) Plot of magnetization distribution. No annihilator was added to the solution. The inversion was assuming a constant magnetic thickness of 1 km along the profile. (c) Schematic representation of the 2-D magnetic source. The body is infinite in the *y* direction. Observation plane is 500 m above sources.

to be optimized. Constrains on the source thickness and magnetization obtained by this deconvolution method may eventually be improved by an independent characterization of the magnetic source to adjust one of these two parameters. Magnetization can be constrained by direct measurements of magnetic properties on rock samples. Variations of the thickness of the magnetic source are, however, at best crudely documented by geological and geophysical data, and in most case simply inferred. A review of recent studies of marine magnetic profiles (Table 1) highlights some results and their limitations: (1) most of these studies (80%) have focused on the characterization of the magnetization distribution assuming a fixed thickness (usually 0.5–1 km) single layered magnetic source; (2) in the few papers that present a model for the magnetic source thickness, this source is assumed to be single layered; results range between 0.1 and 1 km thickness; (3) these few studies of magnetic source thickness are restricted to fast or intermediate spreading ridges and to relatively young crust (2 Ma); and (4) the *Parker and Huestis* [1974] Fourier-based inversion method is used in nearly every case.

[10] We shall now briefly focus on those studies in Table 1 that have inverted magnetic anomaly profiles for the magnetic source thickness. The methods used in these studies deal with the nonlinear inversion of equation (1) by applying a forward iterative method to recover magnetic layer thickness. They are built in one or two steps: (1) the anomaly δT is inverted for the magnetization distribution that is either assumed to be uniform within the source layer [*Lee et al.*, 1996] or is constrained with rock magnetic measurements [*Tivey and Johnson*, 1993] and (2) the magnetic anomaly is modeled to iteratively adjust the thickness of the magnetic layer, starting from uniform thickness initial configuration. Step 2 uses either a Fourier-based scheme [*Parker*, 1973] or a matrix inversion technique [*Lee et al.*, 1996] as initially introduced for gravity by *Tanner* [1967]. In this latter case, equation (1) is linearized then solved by a trial-and-error iterative process. As outlined in Table 1, step 1 is computed with the Parker and Huestis Fourier-based method. This method assumes (1) a constant source layer thickness ($t = z_1 - z_2$) whose upper surface z_1 is defined by the topography, (2) constant magnetization intensity with depth within the magnetic layer, and (3) that magnetization is fixed in the direction of the geocentric dipole. Under these conditions, Parker and Huestis showed that we can find relative values for the magnetization J (these values may be adjusted by adding a magnetization proportional to an annihilator [*Parker and Huestis*, 1973]). A solution consists in constraining this relative computed value with absolute values from NRM measurements on samples from the extrusive layer [*Tivey and Johnson*, 1993]. However, these samples may not be representative of the magnetic layer as a whole. Moreover, *Lee et al.* [1996] have shown that the magnetic layer thickness computed in that way is highly dependent on the value used for *J*. These previous studies therefore provide only relative values for magnetic source thickness. Although these methods may provide robust and spatially continuous results along profiles [*Tivey and Johnson*, 1993; *Lee et al.*, 1996], they rely on theoretical approximations such that magnetization and thickness are not independently determined as illustrated on Figure 1.

2.2. Crustal Magnetization Structure

[11] Let us now briefly review what is generally admitted about marine magnetic sources structure on the basis of magnetic properties measurements, geological studies, and geophysical experiments.

[12] Direct measurements of magnetic properties of abyssal samples have shown that the primary magnetic source of marine anomalies most likely corresponds to the extrusive basaltic layer [*Johnson and Atwater*, 1977; *Bleil and Petersen*, 1983; *Bina*, 1990]. This layer is commonly assumed to correspond with the seismically defined layer 2A [*Talwani et al.*, 1971; *Tivey and Johnson*, 1993], the upper portion of layer 2, whereas the lower portion of layer 2 (layer 2B) is interpreted as a sheeted dikes complex. In terms of magnetic signature, the boundary between layer 2A and layer 2B is usually envisioned as a magnetic transition between highly magnetized extrusives, and weakly magnetized dikes [*Tivey*, 1996; *Shah et al.*, 1999]. The whole of layer 2 is ~2 km thick in normal oceanic crust [*White et al.*, 1992]. Its thickness appears rather independent from the ridge spreading rate [e.g., *Detrick et al.*, 1993; *Babcock et al.*, 1998; *Canales et al.*, 2000] and layer 2A range between 100 and 1100 m thick (see *White et al.* [1992] and *Hooft et*

Table 1. Review of Recent Studies Constraining Magnetic Layer Magnetization and/or Thickness Distribution

Ref[a]	Data Location	Time Coverage, Myr	Deep-Tow?	Magnetic Source Thickness Inferred or Modeled	Techniques
			Fast Spreading Ridges		
1	EPR −20°S	0.06	yes	0.2–1 inferred	upward continuation Parker and Huestis inversion (1 km thick)
2	EPR; Easter/Nazca −25°S to 20°N	zero age	no	0.75–1 km inferred	Parker and Huestis inversion (0.75–1 km) rocks magnetics and geochemical measurements
3	EPR; 28°N, 41°N and 50°N	30–83	no	2.6±1.7 km modeled	use three components field data (least squares method)
4	EPR	2.4	no	1 inferred	Parker and Huestis inversion 3-D (1 km)
5	EPR −19.5°S	0.09	yes	0.2–0.5 inferred	forward modeling NRM from dredged basalts
6	EPR − 9°N	1.5	no	0.15–0.8 modeled	forward iterative modeling Parker and Huestis inversion (0.5 km) NRM dredged basalts
7	EPR − 9°N	0.2	yes	0.1–0.5 modeled	deconvolution
			Intermediate Spreading Ridges		
8	JDF − 48°N	0.78	yes	0.5 inferred	upward continuation Parker and Huestis inversion (0.5 km)
9	JDF−48°N	1	yes	0.1–0.8 modeled	upward continuation Parker and Huestis inversion (0.5 km) iterative forward modeling to get thickness NRM from dredged basalts
10	JDF − 48°N	1	no	∼0.2–2 modeled	multiple-source Werner deconvolution
11	JDF/Gorda ridge− 44°N	2	yes	0.8–1 modeled	(vertical profiling) Parker and Huestis Inversion Geological constrains
12	SEIR	1	no	0.5–2.1 inferred	Parker and Huestis inversion (0.5 km) with variable thickness
13	CIR − 19°S	4	yes	0.5 inferred	upward continuation Parker and Huestis Inversion (0.5 km)
			Slow Spreading Ridges		
14	MAR-Reykjanes	0.78	no	1 inferred	Parker and Huestis Inversion (1 km) NRM dredged samples
15	MAR 15–17°N, 26°N and Gorda ridge (int.)	3	no	1 inferred	forward modeling and Parker and Huestis inversion (1 km) Rocks magnetic measurements
16	MAR	10	no	0.5 inferred	Parker and Huestis inversion (0.5 km)
17	MAR	10	no	1 inferred	Parker and Huestis inversion (0.5 km)
18	MAR 31°–35°S	5	no	0.6 inferred	Parker and Huestis inversion (0.6 km) NRM, FeO/Ti rocks measurements
19	MAR − 24°N	2	yes	0.5 inferred	upward continuation Parker and Huestis inversion (0.5 km)
			no	12 modeled	
20	MAR − 25–27°N	29	no	1 inferred	Parker and Huestis inversion (1 km)
21	MAR − 29°N	2	yes	0.5 inferred	Forward modeling
22	MAR − 30°N	2.58	yes	0.5 inferred	upward continuation Parker and Huestis inversion (0.5 km)
23	MAR-Reykjanes− 57–63°N along-axis		no	0.2–1.5 inferred	Parker and Huestis inversion (0.5 km)

[a]Studies appear in order of publication date for each spreading rate. References are 1, *Perram et al.* [1990]; 2, *Sempéré* [1991]; 3, *Seama and Isezaki* [1991]; 4, *Carbotte and Macdonald* [1992]; 5, *Gee and Kent* [1994]; 6, *Lee et al.* [1996]; 7, *Schouten et al.* [1999]; 8, *Tivey and Johnson* [1987]; 9, *Tivey and Johnson* [1993]; 10, *Hansen and Simmonds* [1993]; 11, *Tivey* [1996]; 12, *Conder et al.* [2000]; 13, *Pouliquen et al.* [2001]; 14, *Sempéré et al.* [1990]; 15, *Wooldridge et al.* [1992]; 16, *Pockalny et al.* [1995]; 17, *Pariso et al.* [1996]; 18, *Weiland et al.* [1996]; 19, *Hussenoeder et al.* [1996]; 20, *Tivey and Tucholke* [1998]; 21, *Allerton et al.* [2000]; 22, *Smith et al.* [1999]; 23, *Lee and Searle* [2000].

al. [1996] for reviews). Seismic experiments conducted across the East Pacific Rise (EPR) show that in layer 2A, there is nearly continuous and has a quasi constant thickness [*Detrick et al.*, 1993; *Babcock et al.*, 1998], although an abrupt increase of layer 2A thickness at the EPR axis has been proposed [*Christeson et al.*, 1996].

[13] Most recent magnetic studies across the EPR or Juan de Fuca (JDF) ridge concern young crust (<1 Ma, Table 1) and focus on the Central Anomaly Magnetic High (CAMH, ∼100 kyr, i.e., 2–8 km wide at these fast to intermediate spreading rates). There are numerous evidences that freshly erupted lavas have very strong magnetizations (∼55 A/m [*Gee and Kent*, 1994]), which decrease drastically over short timescales (∼20 kyr) because of low-temperature alteration [*Gee and Kent*, 1994], to reach values ∼10 A/m after ∼2 Myr [see *Gee and Kent*, 1994]. As this decrease occurs, the contribution of deeper crustal magnetic sources (i.e., sheeted dikes and gabbros) to magnetic field anomalies may increase [*Blakely*, 1983] so that the hypothesis of the extrusives as the sole source of these anomalies may be inaccurate in crust older than 1–2 Myr. Deeper magnetic sources, comprising the whole of layer 2 or even the whole

oceanic crust and part of the upper mantle, have been invoked to explain the shape (i.e., skewness and transition width) of magnetic anomalies measured at sea surface (see review by *Blakely* [1996] or *Dyment et al.* [1997]) and to account for the magnetization intensity of old oceanic crust [*Arkani-Hamed*, 1989; *Wittpenn et al.*, 1989; *Seama and Isezaki*, 1991].

[14] Crustal magnetization models derived from the interpretation of magnetic anomalies are in good agreement with the results from drilling and logging. Intrusive rocks thought to form layer 2B at ODP hole 504B (i.e., diabases from a sheeted dike complex) have mean magnetization values of 1.6 A/m [*Pariso and Johnson*, 1991; *Worm et al.*, 1996] and could contribute up to 45% of the measured magnetic anomalies, provided that they form a 2-km-thick layer [*Pariso and Johnson*, 1991]. *Dunlop and Prévot* [1982] (legs 30, 37, and 45) and *Pariso and Johnson* [1993b] (leg 118 site 735B) have investigated deeper crustal lithologies and have shown that gabbros and serpentinized peridotites could also contribute to magnetic anomalies.

[15] What is known of the seismic and geologic crustal structure at slow spreading ridges suggests that the hypothesis that seismic layer 2A is the primary magnetic source there may be not realistic. Attempts to model the magnetic signal that would be produced by an extrusive layer of the same thickness as layer 2A at the Reykjanes slow spreading ridge show significant misfit both in amplitude and wavelength with the observed anomalies [*Lee and Searle*, 2000]. In addition, numerous geological and nonmagnetic geophysical studies indicate that the lithostratigraphy of the crust and the patterns of alteration in the crust and upper mantle are significantly more complex at slow than at fast spreading ridges [*Cannat*, 1993; *Canales et al.*, 2000]. Geological studies show that variably serpentinized peridotites and gabbros frequently crop out along faults in the axial domain [*Lagabrielle et al.*, 1998] and that crustal accretion is characterized by episodic magmatic events, occurring within a wide (>10 km) axial deformation domain [*Karson et al.*, 1987; *Gente et al.*, 1995]. The crustal structure is therefore much less homogenous than at fast spreading ridges, with a discontinuous magmatic crust and frequent outcrops of deep crustal and mantle-derived rocks. Direct measurements of magnetic properties on rock samples, and magnetic profiles made from a submersible [*Tivey*, 1996] show that the lower crust and upper mantle rocks that are found at the outcrop are able to carry significant induced and remanent magnetizations [*Pariso and Johnson*, 1993a, 1993b; *Nazarova*, 1994; *Oufi et al.*, 1999]. Induced or remanent contributions from deeper crustal levels and from altered peridotites have been proposed to explain the magnetization of nontransformed discontinuities at slow spreading ridges [*Pockalny et al.*, 1995; *Tivey and Tucholke*, 1998]. Yet, papers that have modeled the magnetic source amplitude characteristics near slow and intermediate spreading ridges (Table 1) have so far assumed a continuous and single-layered source, 0.1–1 km thick, that may not be realistic.

3. Continuous Wavelet Transform and Synthetic Examples

[16] We now introduce a wavelet-based method to constrain the source layer thickness and magnetization variations from deep-tow magnetic profiles. The method basically follows the use of complex wavelets as discussed by *Sailhac et al.* [2000]. We assume that the magnetic layer is a series of connected prisms having different height (thickness) and magnetizations (see Figure 2).

[17] *Hansen and Simmonds* [1993] considered a similar model for the magnetic layer and developed a multiple-source Werner deconvolution to estimate its top and basement on the intermediate spreading Juan de Fuca ridge. *Blakely* [1996] pointed out that this technique is sensitive to noise and needs to be applied at several resolutions depending on the depth of sources. This suggests that Hansen and Simmonds approach was successful because they applied it on aeromagnetic data, which are far from the sources (~3 km). As we analyze deep-tow profiles, close to the sources (~0.5 km), we prefer to apply a multiresolution technique which is akin to multiple-source Werner deconvolution but also uses the upward continuation (low-pass filter).

[18] The wavelet-based technique is a multipole source decomposition. When using the wavelet transform, one first applies a correlation analysis to the observed magnetic anomaly resulting in a multipole decomposition of the signal. This provides a space-scale representation (x, a) giving the correlation of the signal with Green's functions of multipole sources at different abscissa x along the profile and depth $-a$ below the data level. Using complex wavelets, this is also an image of the analytic signal, upward continued to the altitude a above the data level. We refer the reader to *Moreau et al.* [1999] and *Sailhac et al.* [2000] for an exhaustive presentation of this technique. Here we recall the main lines.

[19] Let us consider $\delta T(x)$, x being the distance along the profiles and δT being the total magnetic field anomaly associated with an extended source (step, strip, or prism) located at x_0, with mean depth z_0, thickness h, and magnetization J. The continuous wavelet transform of δT is obtained by taking derivatives and upward continuation [see *Sailhac et al.*, 2000, equations (5) and (6)]). Combining the horizontal and vertical derivatives results in the upward continued analytic signal of the field that basically forms the modulus of complex wavelet coefficients $|W\gamma_c\ (x,\ a)|$ [*Sailhac et al.*, 2000, equation (8)]. Parameter γ is the derivative order that controls the number of oscillations in the analyzing wavelets, a is the dilation or altitude of continuation that controls the scale, and x is the translation parameter that gives the position. Thus wavelet coefficients can be computed by using classical programs used in potential field processing [e.g., *Gibert and Galdeano*, 1985]; indeed, the coefficients $|W^1{}_c\ (x,\ a)|$ are classical analytic signals but upward continued at altitude a and multiplied by a. An interesting property related to the analytic signal, is that the moduli of complex wavelet coefficients exhibit maxima whose positions (at the vertical of the sources) are independent of the mean apparent inclination (i.e., of the direction of magnetization and of the azimuth effect which produces the skewness of the magnetic profiles). There is therefore no need, using this wavelet method, to remove the skewness of studied magnetic anomaly profiles (no reduction to the pole). Once computed the wavelet space-scale representation (x, a) of a profile, it can be interpreted by inversions of each modulus maximum line that can be used to characterize local magnetic dipoles or more complex sources [*Sailhac et al.*,

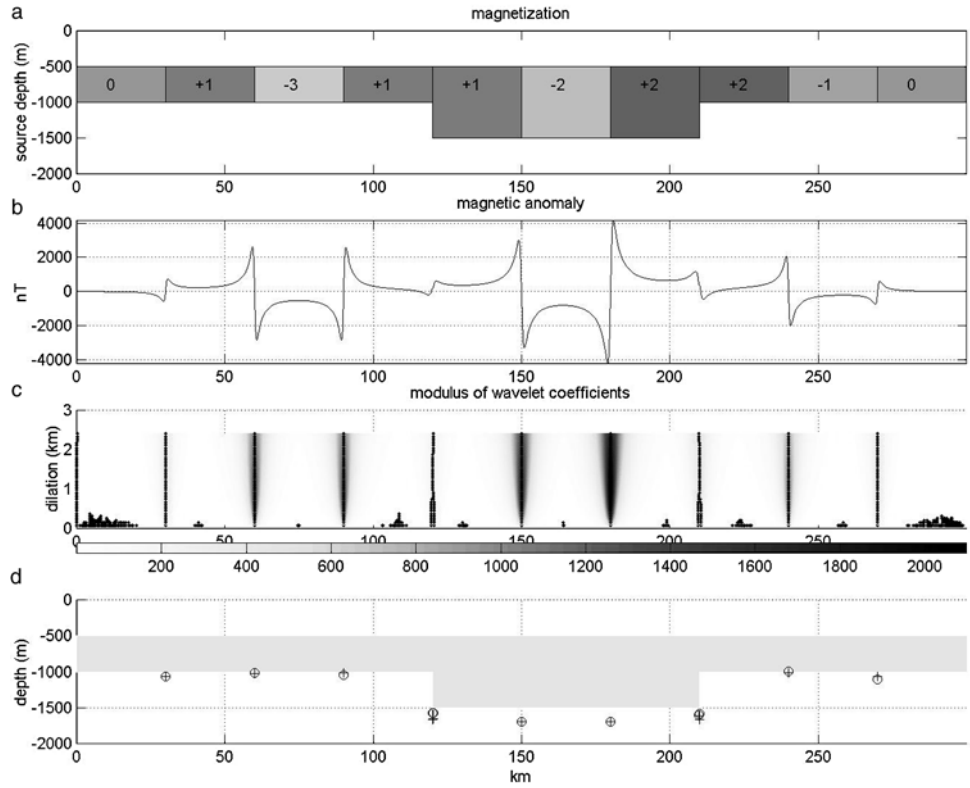

Figure 2. Source height computed using the multipole decomposition method in case of wide (30 km) blocks of uniform magnetization. (a) Synthetic source magnetization and thickness distributions. Darker colors indicate higher magnetization sources (unit is A/m). (b) Synthetic total field anomaly profiles, computed on a plane 500 m above sources. (c) Modulus of wavelet coefficients (units are nT). Solid circles underline the maxima of the modulus. (d) Shaded area showing the synthetic source depth presented in Figure 2a. Open circles are the contact sources heights estimated by the residue of linear regression (see text), i.e., function H with error bar (2σ). Crosses correspond to twice the mean computed depth of the source.

2000]. If the source is a series of connected prisms having different height and magnetization, we can adjust scaling laws of wavelet coefficients to compute height and intensity estimates. For magnetic layer modeling out of deep-tow profiles, we limit the solutions to outcropping sources, those having their height equal to the double of the depth from sea bottom to their middle.

3.1. Source Depth and Source Thickness Estimations

[20] Around a local anomaly source with small height h, wavelet coefficients obey a double scaling law, depending on the actual horizontal and vertical location of the source (x and z_0), on the wavelet dilation a, on an intensity factor k, and on two exponents γ and β [*Moreau et al.*, 1999; *Sailhac et al.*, 2000]. Let us use the logarithm and consider one modulus maxima line at $x^* = x$, this is (for $(z_0 + a) \gg h/2$)

$$\ln(|W\gamma_c(x^*, a)|/a\gamma) = k + \beta \ln(z_0 + a). \quad (2)$$

Exponent γ is the degree of the analyzing wavelet and gives the number of zeros of its real part. It corresponds to the multipole degree for the associated Green's functions. Exponent β is a geometrical index that characterizes the geometry of the source; it is related to the homogeneity degree -N used in Euler deconvolution: $\beta = -(\gamma + N + 1)$. When a source is of finite vertical extent h, one verifies $\beta = -2$ for a magnetization step and $\beta = -3$ for a strip (dike) or a prism [*Sailhac et al.*, 2000]. This scaling law allows us to use the wavelet coefficients to derive the source position, mean depth, and geometry with no a priori information (the intensity contrast is assumed constant within one source, but the value of the intensity contrast, the geometrical index and the position are unknown). The intensity factor $k = \ln(Kh)$ with $K = 2(\sin \mathbf{I}/\sin I')2J$ is related to the inclination of the magnetization vector $\mathbf{I}$, to its apparent inclination I', and to the magnetization J. In the following examples, let us use $K = 2J$.

[21] On the plot of wavelet coefficients (Figure 2c), we observe that the modulus maximum lines of wavelet coefficients converge toward the center or the upper boundary of the sources. This property can be used as a rough estimate for source locations: For small dilations, the lines of maxima point toward the top of the source, while for large enough dilations, they converge to the mean depth z_0.

[22] Equation (2) shows that the mean depth of the source (z_0) can be numerically estimated by a linear regression of the bilogarithmic plot $\ln(|W|/a)$ versus $\ln(a + z_0)$, where z_0 is the a priori depth (the range of z_0 is set by the minimal and maximal dilations). Best fitting values of z_0 and (are selected with a least squares regression misfit from equation

Table 2. Sources Parameters Recovered by the Multipole Decomposition Method for the Synthetic Anomaly Illustrated on Figure 2[a]

Location, km	Depth, m	β	Intensity, A/m	h ($2z_0$), m	H, m	σ(h), m
30	285	−1.91	1.0	570	561	14
60	265	−1.92	4.1	530	518	9
90	260	−1.92	4.1	520	544	9
120	575	−1.71	0.4	1150	1072	84
150	600	−1.95	3.2	1200	1190	5
180	600	−1.95	4.2	1200	1196	4
210	555	−1.70	0.9	1160	1100	86
240	256	−1.95	3.0	514	496	8
270	285	−1.91	1.0	570	602	13

[a]Location is abscissa of source location; depth is source depth (z_0); β is geometric index β of the source (see text); intensity is estimated intensity of the sources (i.e., between two magnetized blocks); h ($2z_0$) is source thickness approximated with $2 \times z_0$; H is source thickness estimated with the function H; and σ(h) is standard deviation of the estimated thickness and depth.

(2). These linear regressions also give the intensity factor k which can be used to estimate the source intensity J once h is known. An assumption is made on the magnetization inclination (see Table 2).

[23] Considering residuals $R(a)$ from equation (2), *Sailhac et al.* [2000] defined a scaling function that allows one to estimate the vertical extent h of simple shaped extended source as the limit for large enough dilations (i.e., $(z_0 + a) \gg h/2$), of:

$$H(a) = 2(z_0 + a)f[R(a)]^{1/2}, \quad (3)$$

where the factor f depends on the shape of the source, it equals 1 for vertical step-like sources (with $\beta = -2$) and $\sqrt{2}/2$ for vertical strip-like sources (with $\beta = -3$). In practice, this limit must be computed as an average over a range of scales involving also small dilations, otherwise the residuals $R(a)$ are too small and the extended source appears as a source which is too small for its vertical extent h to be estimated [*Martelet et al.*, 2001]. For deep-tow profiles, z_0 values as they appear in the previous equations are relative to deep-tow level, not to sea bottom. The actual depths z_0 are obtained by these z_0 values minus the deep-tow to sea bottom distances.

[24] Now, let us consider the modeling of the magnetic layer as a series of magnetized prisms. The source between two prisms of different magnetizations but same thickness is a contact source which intensity is the magnetization contrast and which height is the thickness. The source between two prisms of same magnetization but different thickness is a contact source which height is the thickness variation and which intensity is the magnetization (Figure 2). For both cases, the factor f equals 1.

[25] Furthermore, in case of different magnetizations but same thickness, the estimated thickness h can be related to the depth z_0 via the relation $h \sim 2z_0$. Without using this latter relation, *Martelet et al.* [2001] estimated h as the average of $H(a)$ by minimizing the variance of $H(a)$ in the three-parameter space of (z_0, k, β). Now using the same three-parameter space, we minimize the squares of $H(a) - 2z_0$ so that the resulting depth z_0 allows to fit the new relation $h \sim 2z_0$ that we expect for the deep-tow magnetic profiles. The uncertainty of the estimated thickness h can be roughly estimated by using either the final value of the squares of $H(a) - 2z_0$ or the difference between the mean value of $H(a)$ and $2z_0$ (no precise assumption on the parameter distributions has been considered in this paper).

3.2. Synthetic Sources

[26] In the following sections, we tested the sensibility of the wavelet based method to changes in the parameters of the magnetized layer, namely its geometry (i.e., its thickness, width, and depth) and its magnetization, and we considered the effect of noise. We address these issues through the analyses of anomalies produced by synthetic magnetic profiles.

[27] The source is a magnetic layer made of blocks with different thickness, width, and magnetization contrasts such that magnetization intensities vary at frequencies corresponding to the timescale of geomagnetic field reversals (chrons and subchrons, $>10^5$ years duration), and to the timescale of shorter-lived geomagnetic events ($<10^5$ years). Thus this magnetic layer is made of a series of magnetization contrasts, each being a step-like source located right at the edge of a magnetization block; the geometry for each border can be characterized by a shape index $\beta = -2$ [*Sailhac et al.*, 2000]. To compute the resulting synthetic total field anomalies, we have chosen a sampling interval of 80 m (similar to that of the CIR deep-tow data). The observation plane was set at 0.5 km above the sources (comparable to the average altitude of the CIR deep-tow profiles). All synthetic magnetic anomaly profiles have been computed at the pole for clarity (although using complex wavelets involves the use of analytic signal and avoids the need of reducing to the pole). Wavelet transforms have been computed at order $\gamma = 1$, and for a large range of dilations (or upward continuation altitudes) with 100 m increments, comparable to the horizontal data spatial sampling. A code has been developed to automatically scan the data along lines of modulus maxima of the wavelet transform coefficients and determine the best scale or dilations range to use for each source (using a trial procedure similar to that used by *Martelet et al.* [2001]). Thus we have tested different maximum values for the upward continuation altitudes or dilations (a_{max} = 1.6, 2.4, 3.2, 4, 4.8 km). We show on Figure 2 and Table 2 the results obtained for a model built with homogenous magnetization blocks 30 km wide and 500 to 1000 m thick, using a maximum dilation a_{max} of 2.4 km. This maximum dilation was found to provide the best fit between the calculated source thickness, and the actual source thickness of the model. When a_{max} is too small (i.e., when the ratio $(z_0 + a_{max})/(h/2)$ is too small), the upward continuation altitude is too small with regard to the source thickness. The computed mean depth of the source is then underestimated, corresponding with a location close to the top of the source, while the source height is not determined or is determined with large error bars.

3.2.1. Sensibility of the Method to Changes in the Geometry of the Magnetized Layer

[28] Concerning the sensibility of the method to source thickness variations, the error on estimated height remains <20% for source layer thickness of 50–1000 m and for maximal dilations of 2.4, 3.2, and 4.8 km. At dilations <2.4 km, sources 1000 m thick are not resolved, and we loose accuracy for thinner sources (Figure 3). A maximum dilation a_{max} = 2.4 km should provide a good intermediate value for data acquired ~500 m above the sources with a

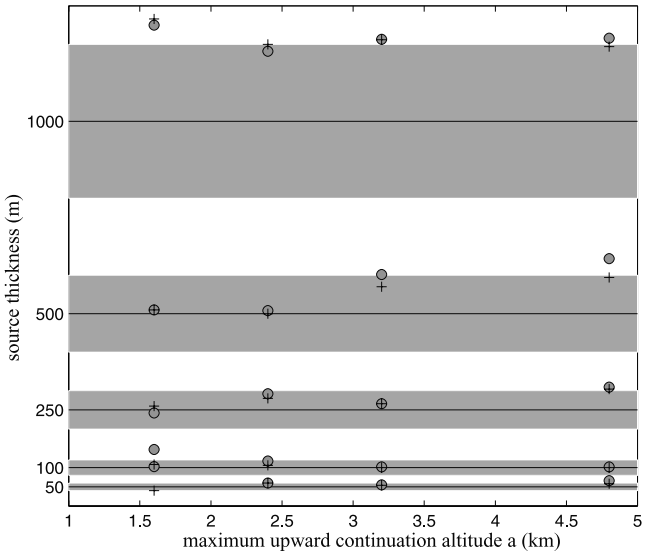

Figure 3. Influence of the maximal upward continuation level (or maximal dilation a) of the wavelet transform on the accuracy of block thickness computations by multipole decomposition. Tests have been done on 50, 100, 250, 500, and 1000 m thick sources and for 1.6, 2.4, 3.2, and 4.8 km maximal dilations. Open circles are the calculated thicknesses of the sources. Crosses correspond to twice the mean computed depth of the source. Solid lines correspond to the actual thickness of the model source. Grey envelops show the 20% confidence range.

sampling interval of 80 m (i.e., acquisition parameters similar to the CIR data). Figure 2 illustrates two possible configurations with respect to changes in source intensity and thickness: in the first configuration (at 120 and at 210 km), the source layer thickness varies but the magnetization remains unchanged; in the second configuration (every other blocks), the source thickness remains the same, but the magnetization varies. In both cases, we recovered the source thickness with an accuracy of 1–20% (Figure 2). Modulus maximum lines in Figure 2 do not show a noticable curvature at small dilations (see Figure 4 for comparison), and there is only a slight difference between the $2z_0$ approximation for h (crosses in Figure 2d) and the value obtained using function $H(a)$ (open dots). This difference can be used to measure the quality or misfit of our estimates. Indeed, it is maximum over the edges of magnetized blocks showing almost the same intensity but a contrast in thickness (actually this is a place where sources are not outcropping steps). We tested the sensibility of the method to intensity variations and found that we were able to resolve intensity contrasts down to 0.2 A/m.

[29] A geological analogue to the wide blocks model (width/height ratio >10, Figure 2) would be a magnetic source layer with wide, homogeneously magnetized intervals that have recorded the geomagnetic field intensity over long periods. On the contrary, a geological analogue to the narrow-blocks model (width/height ratio < 10; Figure 4) would be a magnetic source layer with closely spaced lateral changes in magnetization resulting from field intensity fluctuations with short-lived geomagnetic events [e.g., *Valet and Meynadier*, 1993; *Kok and Tauxe*, 1999]. We investigated source thickness variations recovered from magnetic anomalies generated by a sequence of narrow magnetized intervals 1–5 km wide (i.e., ~50 kyr to 230 kyr long intervals for CIR spreading rate); such sources represent a filtered record of short-time variations of the geomagnetic field intensity. Tests carried out for this range of block widths show that for blocks narrower than ~5 km (i.e., for a width/height ratio of 10; Figure 4) the accuracy of layer thickness determinations falls down below 30 and 40% for 2-km-wide block models. Figure 4 shows that the multipole decomposition method can only partly handle anomalies created by small (0.2–0.5 nT) closely spaced magnetization contrasts and that complete sources determination will depend on the horizontal magnetization sequence. While a series of lines of wavelet transform modulus maxima reflects a series of single magnetization contrasts in the case of large blocks, a single maxima line may reflect a set of overlapping contrasts playing as a single complex source. Graphically, we can observe curved lines of maxima instead of straight lines, even at small dilations. This phenomenon has been illustrated by *Sailhac et al.* [2000] with a buried prism of height h and width l at depth z_0: it appears as a local source having a single line of maxima as long as $(z_0 + a) \gg h/2$ and $(z_0 + a) \ll l/2$, whereas at smaller dilations there are two lines of maxima pointing to the borders of the prism. Thus, when the depth z_0 is relatively large, values of $z_0 + a$ are large even at small altitudes a, and a narrow succession of magnetization contrasts is seen as a single local source even at small altitudes.

[30] Applying wavelet transform to the interpretation of CIR deep-tow profiles, we expect to resolve wavelength larger than ~4–5 km only. Therefore, although the multipole decomposition method provides acceptable results when applied to closely spaced magnetization blocks (Figure 4), thickness estimates are more accurate for sources constituted of a pattern of large magnetization blocks (Figure 2). The method is badly fitted to characterize blocks that have their width comparable to or smaller than their thickness or whose sizes are larger than the deep-tow to seafloor distance.

3.2.2. Sensibility of the Method to Changes in the Intensity of the Magnetic Field

[31] We tested the sensitivity of the wavelet analysis to realistic magnetizations variations, using a synthetic magnetic anomalies profile (Figure 5) in which a constant thickness (500 m) magnetized layer presents magnetization variations proportional to the *Valet and Meynadier* [1993] intensity variations model. In this model, the initial intensity curve has been resampled to take into account the CIR half spreading rate and the data increment. We kept the same parameters (observation altitude, increment of observation stations) than for the two previously discussed synthetic profiles.

[32] The mean magnetic layer thickness calculated for the whole profile is of 545 m, with minimum values of 260 and 840 m, respectively. Depths of the magnetized layer basement are determined with good accuracy at the level of the significant changes of magnetization, i.e., for the main chrons and subchrons boundaries (Figure 5d). These changes are associated to wavelet coefficients of high amplitude. In comparison, the modulus corresponding to lower intensity contrasts have lower amplitude and the accuracy on the estimated depth of the magnetized layer basement decreases

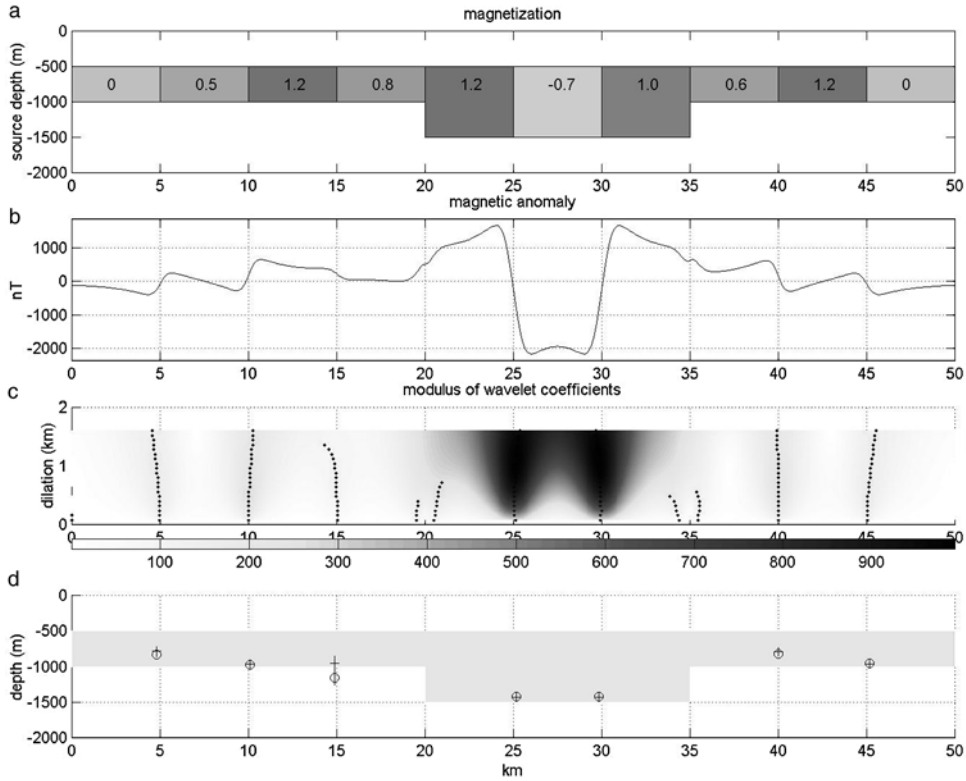

Figure 4. Source mean depth and vertical extension computed using the inversion of wavelet coefficients for narrow (5 km) uniformly magnetized blocks. (a) Synthetic source with narrow magnetized blocks. Darker shading indicate higher magnetizations. (b) Synthetic total field anomaly profiles. (c) Modulus of wavelet coefficients (units are nT). Solid circles mark the location of maxima lines of the modulus. (d) Shaded area showing the synthetic source depth presented in Figure 4a. Open circles are the source thicknesses estimated using function *H*. Crosses correspond to twice the mean computed depth of the source. Error bars (2σ) are similar for estimated mean depth and thicknesses.

(Figure 5). Thus the wavelet method can not properly resolve anomalies associated to short-term (i.e., <5 km) small changes of magnetizations. However, in good agreement with the results developed in section 3.2.1, the calculated average magnetic basement depth is consistent with the initial model at longer spatial scale (>∼5 km).

3.2.3. Sensibility of the Method to Noise

[33] We have not specifically tested the effect of noise in the data, compared to the uncertainties caused by short-scales variations in the thickness and/or the magnetization of the source layer. However, we the results of previous studies on the effect of noise onto the accuracy of wavelet-based model parameter estimates suggest that this effect may be negligible [*Moreau et al.*, 1999; *Sailhac*, 1999; *Martelet et al.*, 2001]. In these previous studies, scaling law fitting of wavelet transform modulus maxima is applied over a range of scales such that the ratio of signal to noise is maximum. In practice [see *Martelet et al.*, 2001], the range of scales is selected automatically to fit a simple scaling law (equation (2)) that corresponds to a local homogeneous source at depth z_0. This search for the best range of scales starts with all scales below 2.4 km. Then the more complex scaling law (equation (3)) is adjusted over the resulting range of scales, where all depths between $0.9z_0$ to $1.9z_0$ are tested. On the basis of our experience, we consider that this procedure performs well with actual noisy data from deep-tow acquisitions similar to that of the CIR, with data uncertainties of some nanoteslas acquired at ∼500 m above the sources with variable thickness of 50–1000 m.

4. Source Thickness Determination Using Deep-Tow Marine Magnetic Profiles

[34] After tests on synthetics, we test the wavelet-based technique on one deep-tow profile in a well-known region across the JDF ridge. Then we apply it to deep-tow profiles of the CIR.

4.1. Test on Juan De Fuca (JDF) Ridge Deep-Tow Profile

[35] The deep-tow profile is ∼20 km long and shifted on the left about the JDF ridge axis (Figure 5). It covers ∼300 kyr on the east ridge flank (half spreading rate ∼40 km/Myr). We choose this profile for three reasons: (1) thickness variations of the magnetic sources have been previously estimated from this profile using a method derived from the *Parker and Huestis* [1974] approach [*Tivey and Johnson*, 1993], (2) seismic experiments have provided constrains for the layer 2A thickness along this profile [*White and Clowes*, 1990], and (3) although the JDF ridge spreads about twice as fast as the CIR, both ridges have comparable geophysical signatures (bathymetric, gravimetric and magnetic).

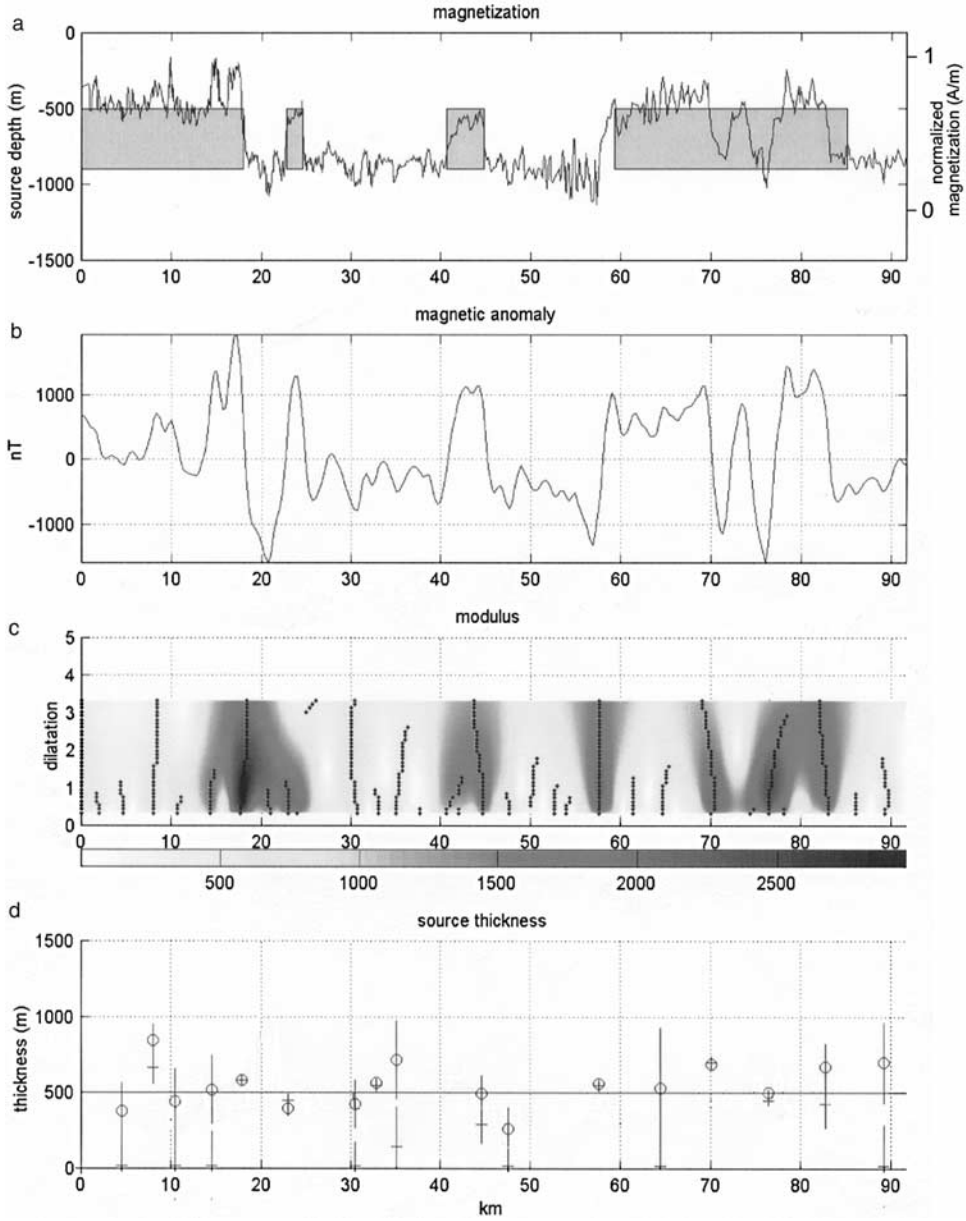

Figure 5. Source mean depth and vertical extension computed using the inversion of wavelet coefficients for magnetization variations proportional to the intensity variations suggested by *Valet and Meynadier* [1993]. (a) Synthetic source with magnetization (thin solid line) following the paleointensity curve (with normalized amplitude). Shaded area shows geomagnetic intervals of normal polarity (Brunhes, Jaramillo, Olduvai, Matuyama) and the initial model depth and thickness. (b) Synthetic total field anomaly profiles, computed considering the CIR spreading rate. (c) Modulus of wavelet coefficients (units are nT). Solid circles mark the location of maxima lines of the modulus. (d) Solid line at 500 m shows the initial source basement. Open circles are the source thicknesses estimated using function *H*. Crosses correspond to twice the mean computed depth of the source. Error bars (2σ) are similar for estimated mean depth and thicknesses. The mean estimated depth of the magnetized layer basement is 545 m (standard deviation of 140 m).

[36] The results of the multipole decomposition method for the JDF profile are presented in Figure 5. They are a discrete series of thickness estimates with a narrow spacing of 2∼4 km at the location of strong modulus of the wavelet coefficients. This sampling focuses on the major changes in the amplitude of the magnetic field anomalies. Indeed, wavelet coefficients are analytic signals that are defined from gradients of the magnetic field. Sources detected by the technique are characterized by a geometrical index of $\beta = -2$ (which corresponds to a step-like geometry) and to thickness estimates nearby the double of their depth estimates (which corresponds to outcropping). Errors bars of these thickness estimates on the JDF are very moderate; this comforts this multipole decomposition technique, at least on

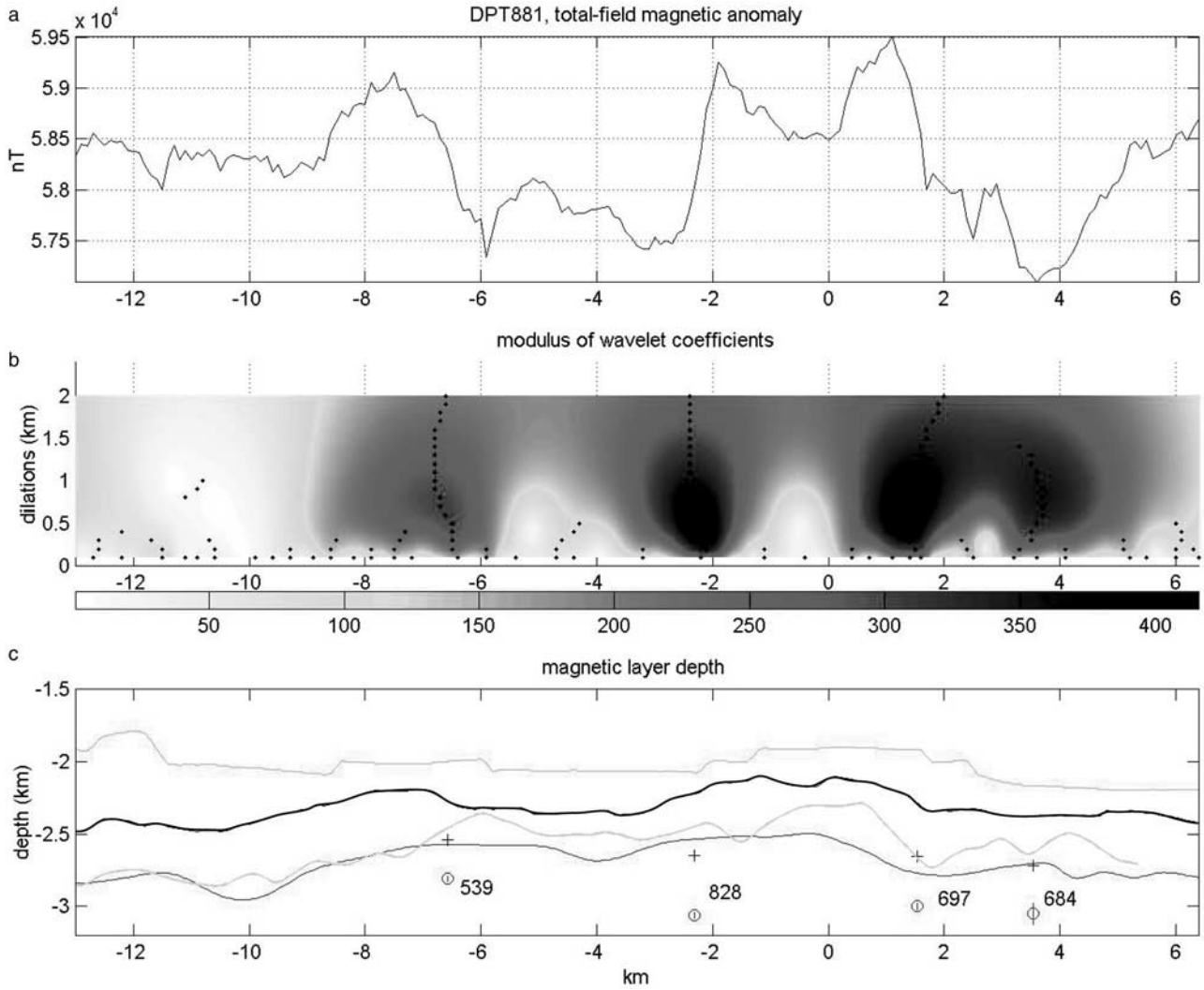

Figure 6. Multipole method applied to JDF deep-tow magnetic profile. (a) Total magnetic field across the ridge. In abscissa is the distance along the ridge. (b) Modulus of the wavelet coefficients of the magnetic profiles (units are nT). Solid circles single out modulus maxima. (c) The thick solid line is the bathymetry along the profiles, and the top solid line is the magnetometer altitude. Open circles are the magnetic layer basement calculated from the multipole method (function *H*) and solid crosses show the source mean depth estimated with z_0. Gray line shows magnetic layer thickness obtained by *Tivey and Johnson* [1993], and thin bottom solid line is the seismically defined basement of layer 2A.

the basis of an accuracy criteria. The average source thickness obtained along the profile using the step-shaped source approximation is 690 m. This is about twice the average thickness obtained for the magnetized layer by *Tivey and Johnson* [1993] (285 m). This is also more than the thickness determined, with uncertainties that reach 30–35% beneath the ridge axis, for seismic layer 2A in the same region [*White and Clowes*, 1990].

[37] The difference between magnetic layer thicknesses obtained with the wavelet method, and with the Fourier-based method used by *Tivey and Johnson* [1993] could be due to the effect of a two-layered magnetic source. The upper layer, which would be fully determined through the Fourier-based method (see section 2.1), would exhibit short-lived intensity contrasts (i.e., narrow magnetization blocks), while the lower layer would have less numerous, wider magnetization blocks and would be detected using the multipole method. To test this hypothesis, we realized two very basic two-layered synthetic models (Figure 6). In the first model (*a*), the upper layer is comprised of narrow magnetization blocks (5 km wide; similar to the sequence presented in Figure 4) and the lower layer is made of blocks twice wider (10 km wide). In the second model (*b*), we have the reverse source layer configuration. In both models, the two layers have constant and identical thickness (250 m); the upper magnetized layer has a thickness comparable to the one estimated for layer 2A along the JDF profile. We calculated the anomalies created by these two models with parameters similar to our previous synthetic models and applied the wavelet-based inversion method. For model (*a*), the magnetic signal includes an additional short-wavelength signal created by the upper, narrow blocks layer. Results of the multipole decomposition are strongly perturbed by this upper, narrow block layer wherever the contribution of the

upper layer to the total anomaly is dominant (see, for example, the source located at 15 km). In contrast, the multipole decomposition gives good estimates of the total thickness of the source wherever the intensity within the bottom magnetized layer is stronger than the one of the upper layer (see sources located at 5 and 10 km). For model (*b*), the magnetic signal is dominated by the longer wavelength generated by the wide magnetization blocks within the upper layer. In this case, the multipole decomposition detects the upper layer thickness with good accuracy, ignoring the bottom source layer contribution. Depending on the respective magnetization intensities of both layers (here, we considered magnetization ratio of 1.5 and 2 between the top and bottom layer), the multipole method handles alternatively the two magnetized layer thickness, switching between 250 (thickness of the upper layer) and 500 m (total thickness of starting source).

4.2. Application to Central Indian Ridge (CIR) Deep-Tow Profiles

[38] We analyze three deep-tow magnetic profiles centered about the CIR ridge axis and extending to ~3.5 Ma crust on each flank. Wavelet transform is applied to raw data (Figure 8a) without reduction to the pole. The altitude of the magnetometer is used to fix the distance to the top of the magnetic layer. Given the CIR spreading rate, tests on synthetic sources (section 3) have shown that the multipole method is in principle well fitted to resolve sources that reflect thickness and/or intensity variations averaged over 10^5 kyr windows. We have calculated wavelet coefficients up to a 2.4-km continuation altitude, a value determined empirically using synthetic examples built with the same data spacing and recording altitude than the CIR data (this yields a sampling interval of 80 m for the scales; Figure 8b).

[39] In the results of the multipole method (Figures 8b and 8c), the shortest distance between two successive sources is ~2 km (i.e., ~80 kyr). Average source thicknesses determined for the CIR profiles are ~650 m for profile A ([1140–116 m]; Figure 8), 600 m for profile B ([1228–156 m]; Figure 9), and 480 m for profile C ([868–239 m]; Figure 9). These thickness averages suggest that there is a moderate increase in magnetic layer thickness from north (profile C) to south (profile A) along the ridge. Instead of averages over the whole profiles, we calculated sliding averages over 1-Myr windows along profiles A, B, and C that show that there are no systematic across-axis variations in the magnetic layer thickness estimates. There is therefore no indication for variations of the magnetic layer thickness with the age of the crust. However, along profile A we observe a mismatch between the axial region (a region ~30 km wide, centered on axis and characterized by smaller magnetic layer thickness estimates) and older areas. This suggests that axial magnetic sources along profile A could be either heterogeneous in magnetization or truly thinner than off-axis sources (Figure 7). In the westernmost part of profile B (Figure 9, 0–30 km), source thicknesses are poorly recovered. This area is characterized by a smooth magnetic signal with moderate gradients and is therefore poorly fitted for the wavelet technique, which yields results for the local maxima of analytic signals. *Pouliquen et al.* [2001] showed that in contrast with the rest of the study area, the magnetic anomalies in this westernmost region are poorly fitted by a synthetic profile calculated with a constant thickness magnetic layer and with magnetization proportional to paleointensities.

5. Discussion

5.1. Influence of Source Intensity and Thickness Variations on Short-Wavelength Magnetic Anomalies

[40] One aim of our study was to evaluate the contribution of short-scale magnetic layer thickness variations to the magnetic anomalies, using constrains from the wavelet technique. In a recent study, *Schouten et al.* [1999] argued that at least for very recent times (i.e., the CAMH), variations of near-bottom anomalies at the EPR primarily reflect variations of the volume of extrusive, assimilated to seismic layer 2A. In an earlier study of the CIR deep-tow profiles [*Pouliquen et al.*, 2001], we showed that recorded anomalies were well matched with a constant thickness magnetic layer model, using magnetization intensity variations as constrained by paleointensities from magnetostratigraphic studies [*Valet and Meynadier*, 1993; *Kok and Tauxe*, 1999]. We reexamine this model, particularly for the most recent portions of each profile, using a forward modeling assuming wavelet-based magnetic layer thicknesses. As in our earlier model, we assume that the magnetization of the source is proportional (with a 20 A/m maximal value) to paleofield intensities estimated by *Valet and Meynadier* [1993]. Because our purpose here is not to discuss the validity of published paleointensity models, we have used a single record, the *Valet and Meynadier* [1993] one, to constrain the magnetization of the source in our forward model. Morerover, given the sensibility of the method to width/height ratio of the sources (see section 3.2), sources associated to short-term (<~2 km) intensity variations will not be analyzed in term of thickness. It is therefore likely that using anyone of the available paleointensity models [e.g., *Kok and Tauxe*, 1999] would lead to similar results.

[41] In our forward model, we neglect the effect of weathering on basalt magnetization [*Schouten et al.*, 1999]. This simplification partly justified by the fact that this weathering effect is thought to occur very rapidly, so that the magnetization rapidly reaches a stable background level (in ~150 kyr with a time constant of 20 kyr [*Gee and Kent*, 1994]). Resulting magnetization profiles are stretched in order to match the principal reversals identified along each profile (Brunhes, Jaramillo, Olduvai, and Gauss boundaries) that we use as tie points [*Pouliquen et al.*, 2001]. Synthetic magnetic anomalies are computed for a constant observation depth (2 km below sea level, just above the topography) and compared to the observed profiles upward continued to the same level [*Pouliquen et al.*, 2001].

[42] Figure 10 shows the results of this computation for profile A. Models for profiles B and C are similar. Magnetic anomaly profiles derived on the one hand for a constant thickness source with varying magnetization, and on the other hand for a combination of source intensity and source thickness variations (as derived from the wavelet transform) show comparable RMS misfit with the actual data: 191 nT along profile A for the constant thickness model and 190 nT for the wavelet transform model. By comparison to the constant thickness model, the wavelet-based variable magnetic layer thickness forward model therefore does not improve the fit with the data.

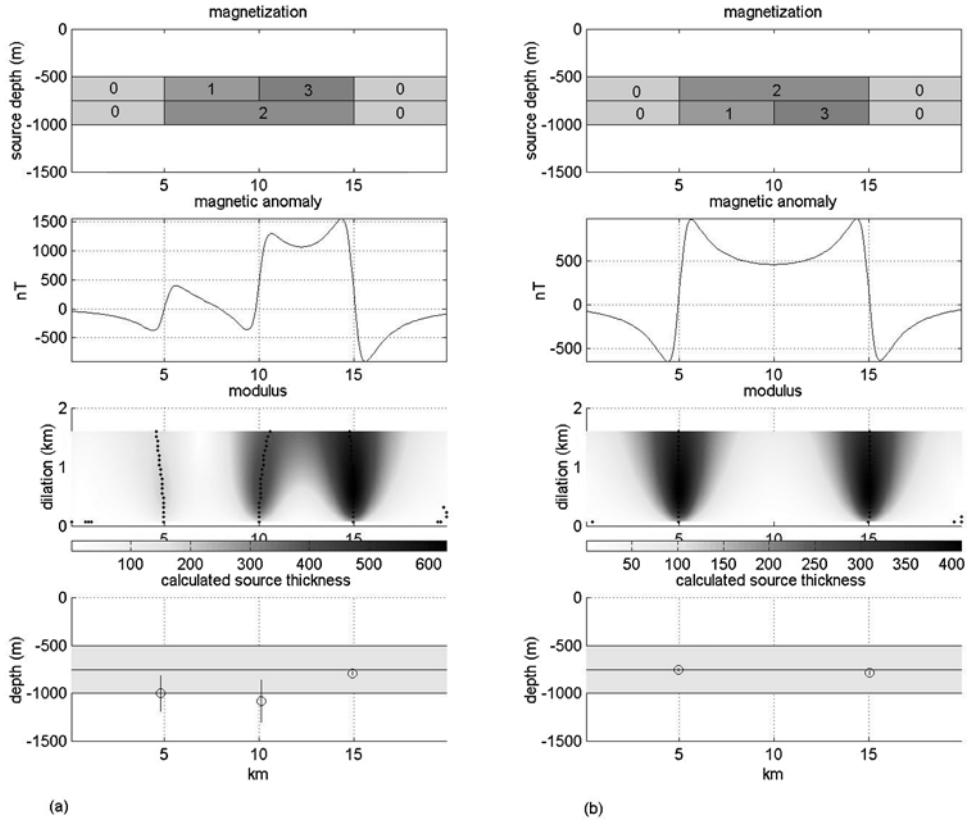

Figure 7. Multipole method applied on two-layered sources. (a) Upper layer comprises narrow magnetization blocs and lower layer wider blocs (10 km wide). Darker shading indicate higher intensity. (b) The source layers are inversely distributed. (top) Starting model. (second panel) Computed anomaly. (third panel) Modulus of the wavelet transform coefficients. Solid circles underline modulus maxima. (bottom) Open circles are the source thicknesses estimated using the multipole decomposition method with error bars. Gray area recall the starting model top and basement depths.

[43] Magnetic anomaly profiles derived from these two forward models do, however, show significant misfits (up to 300 nT; Figure 10b). Two types of magnetic sources generate significant misfits (>100 nT): (1) moderate (∼<100 m) variations of the thickness of the magnetized layer, coupled with strong intensity contrasts (for example, at the Brunhes/Matuyama chrons boundaries and off-axis at the Gauss/Matuyama boundaries in Figure 10), (2) strong source thickness variations (∼≥200 m), coupled with moderate intensity contrasts (for example, within 15 km of the axis in Figure 10). Type 1 and type 2 magnetic sources are similar with respect of the contrast in total magnetization, i.e., the product of the magnetic source height h and magnetization J. Using our forward model, we can therefore predict that thickness variations of the magnetized layer will have a significant effect on the magnetic anomaly record if they correspond with contrasts in total magnetization in excess of a critical value of ∼200 m. We also show that our wavelet-based magnetic source thickness variations for the CIR profiles have the potential to enhance or attenuate the amplitude of the anomalies caused by changes in magnetization but do not induce short-term anomalies, except within 15 km of the ridge axis.

[44] Our results obtained both on synthetic and observed data therefore suggest that variations of the magnetic layer thickness across the CIR are not the cause of the short-wavelength (0.05 to ∼0.2 Myr) anomalies recorded in the deep tow profiles but that the anomalies primarily reflect intensity variations. This result must be tempered for the Brunhes chron (780 kyr duration), where magnetic layer thickness variations alone may be the cause of fairly substantial short-scale magnetic anomalies (>100 nT).

5.2. Origin of Magnetic Layer Thickness Variations and Implications for the Structure of the Magnetic Source

[45] Magnetic layer thicknesses calculated with the multipole wavelet decomposition method are spaced by 4−5 km wide on average, both for the JDF profile and for the CIR profiles (see Figures 6, 8, and 9) Figure 10. We have shown that this spacing is largely inherent to the method, given the acquisition altitude of the profiles, the data spacing and the dilations (see section 3.2). As a consequence, the method cannot resolve magnetic layer thickness variations occurring over shorter spatial-temporal scales. One must also keep in mind that the inversion of deep-tow magnetic anomalies yields multiple solutions. In order to solve this inverse problem, one must make assumptions. One particular assumption, which is made in both the wavelet-based and the Parker and Huestis-based inversion methods, is that there are no vertical heterogeneities of magnetization within the source layer. This is unlikely to be the case in the actual

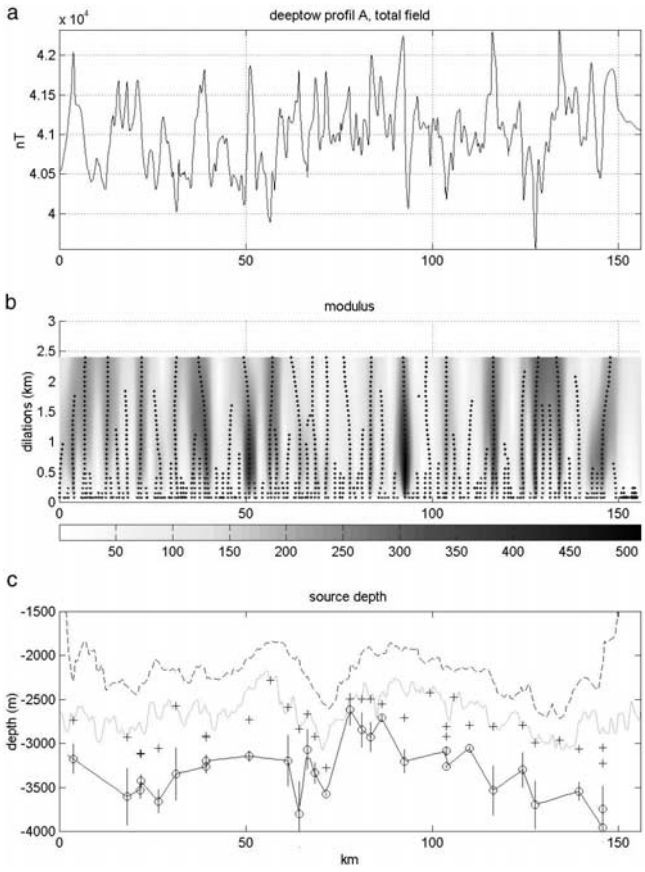

Figure 8. Sources thicknesses along CIR deep-tow profile A. (a) Total magnetic field anomaly. (b) Modulus of wavelet transform coefficients (computed by multistrip method) of magnetic anomaly (in nT). Solid circles locate the maxima lines. (c) Solid dashed line is the altitude of measurements; gray line is the topography. Open circles are the magnetic layer basement calculated from the multipole method (function H), and solid crosses show the magnetic source mean depth estimated with z_0.

source of marine magnetic anomalies, and this simplification could induce apparent variations of the estimated thickness of the magnetized layer. Because of these limitations, the results of inversion methods should be used with caution. In the next paragraphs, we nonetheless discuss the geological processes that could cause magnetic layer thickness variations in the range of those computed for the JDF and CIR profiles.

[46] Variations of the magnetic layer thickness over across-axis distances of only a few kilometers are unlikely to be due to variations in the volume of magma supplied to the ridge as a whole, because such variations should occur over longer periods ($\sim 10^6$ years). There is no trend in the variations of estimated magnetic layer thickness at this timescale in the deep tow profiles we have studied.

[47] The upper portion of the oceanic crust is formed by lavas that can flow over substantial distances [*Macdonald et al.*, 1989; *Hooft et al.*, 1996]. The extrusive layer is therefore probably comprised of successive lava flows representing eruptions that occurred over significant durations. *Hooft et al.* [1996] presented a stochastic model for the emplacement of layers 2A and 2B at the EPR and proposed that the region of overlapping lava is ~2 km wide on average, i.e., that lava ages may be 30–70 kyr younger than those estimated by using the spreading rate and distances from the axis. In this model, the extrusive layer is made of two units: the upper unit comprises thick flows that have spread over large distances and may have erupted at off-axis vents, and the lower unit is made of older, thinner and shorter flows erupted on axis. *Macdonald et al.* [1989] have shown on the EPR that large volumes of magma can be emplaced quickly over distances of a few kilometers (up to 18 km) and fill off-axis depressions and fissures. Hence assuming that extrusives are the principal source of the observed magnetic anomalies, short-scale magnetic layer thickness variations can reflect a topography-controlled distribution of lavas flows around the eruption sites.

[48] The persistence of a readable magnetic lineations pattern then implies that the overlap of successive lava flows occurred over periods sufficiently short to allow for a record of time variations of the field intensity without mixing with older magnetic signatures. However, the western end of CIR profile B (corresponding to the Gauss chron, see *Pouliquen et al.* [2001]) could be an exception. There, source thickness variations are poorly constrained because deep-tow magnetic anomalies are characterized by a smoothed signal with moderate gradients (Figure 9). The weak magnetic anomaly gradients observed in that part of profile B suggest that the source is made of successive lava flows that spread over large distances, thus producing a smoothed magnetic signal. These anomalies are poorly fitted by a model built with magnetization proportional to paleointensities [*Pouliquen et al.*, 2001]. The magnetic layer in this area could be thicker than average, possibly as a consequence of enhanced volcanism resulting from the interaction of the Rodrigues hot spot with the CIR [*Dyment et al.*, 1999; M. Maia, personal communication, 2000].

[49] Oceanic magnetic sources must accommodate a paradox: on the one hand one expects the emplacement history of these magnetic sources to be complex: overlapping basalt flows, off-axis eruptions, postdeposition tectonic disruption, and changes of the rock magnetic properties with time and degree of alteration; and on the other hand, theses magnetic sources are found to preserve a good record of geomagnetic field past intensities, even for short time periods [*Gee et al.*, 2000]. Over the ultrafast spreading East Pacific Rise, the magnetic crustal record inferred from near-bottom magnetic anomalies and from magnetic measurements on basalt samples, appears to reflect geomagnetic field intensity variations that have a very tight temporal resolution [*Gee et al.*, 2000]. In order to preserve such a short-wavelength signal, there must be very limited noise introduced through magnetic crustal layer emplacement. Even a lateral overlap of ~2 km for lava flows at the very fast spreading EPR [*Hooft et al.*, 1996] should limit the temporal resolution to ~20 kyr for the magnetic record of extrusives and would not be consistent with the results of *Gee et al.* [2000] on closely spaced basalt samples. A possible explanation, although it does not account for the paleomagnetic results obtained on basalt samples at the EPR [*Gee et al.*, 2000], is to consider that the observed high temporal resolution magnetic record is carried by the dikes that feed the lava flows. Dikes can carry a stable remanent magnetization [*Pariso and Johnson*, 1991; *Dunlop*

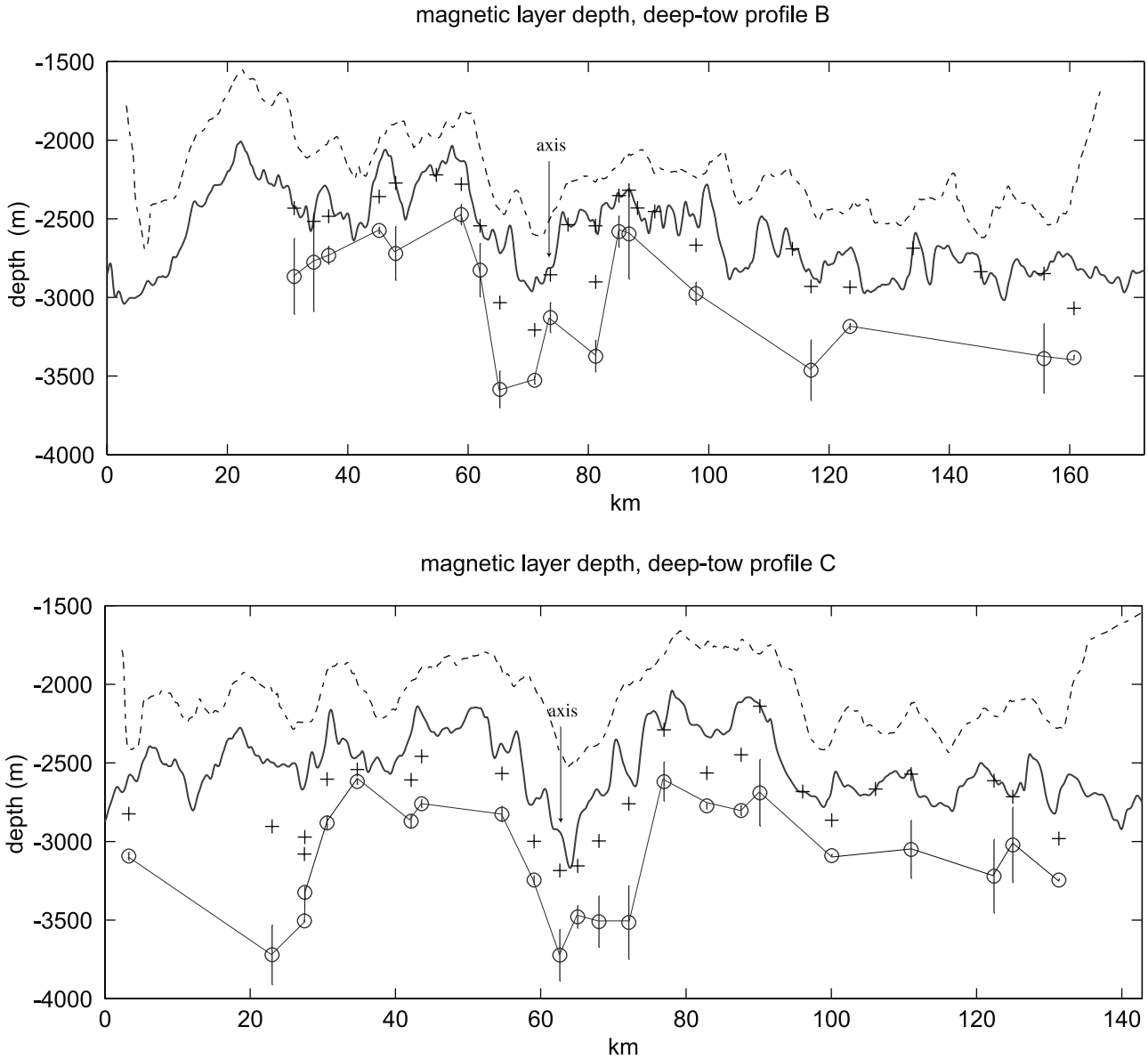

Figure 9. Magnetic layer basement estimation for CIR deep-tow profiles B and C. Dashed line is the altitude of measurements, and solid line is the topography. Open circles are the magnetic layer basement calculated from the multipole method (function H), and crosses show the source mean depth estimated with z_0.

and Prévot, 1982] and are expected to be intruded mostly in a narrow region at the axis. It is unlikely that the magnetic record carried by dikes that lie more than 500 m below seafloor may cover the signal produced by the upper lavas section, and generate an observable signal with short wavelengths $<\sim 3-5$ km [*Blakely*, 1996]. Hence it appears unlikely that dikes from layer 2B contribute significantly to the very short wavelength (<150 kyr at the CIR) magnetic anomalies observed with a deep-tow some 500 m above seafloor. However, shallower dikes that cut through preexisting flows in the upper crust to feed the more recent eruptions could contribute to these short-wavelength anomalies.

[50] At the JDF ridge, discrepancies between the magnetic layer thicknesses calculated with *Tivey and Johnson* [1993] method and the multipole wavelet method, respectively, are systematic. The former yields magnetic layer thicknesses of $\sim 200-300$ m, comparable to the thickness of the seismically defined layer 2A in the area [*White and Clowes*, 1990]. The multipole method yields larger thickness values of ~ 700 m. We have shown that the results of the two methods can be reconciled if the magnetic source is comprised of two layers. The upper layer would exhibit short-lived intensity contrasts (i.e., narrow magnetization blocks), while the lower layer would have less numerous, wider magnetization blocks and would be detected using the multipole method provided that his magnetization was stronger (with a ratio of 1.5–2) than that of the upper layer.

[51] This two-layer hypothesis is difficult to reconcile with the generally accepted idea that the extrusive basalts

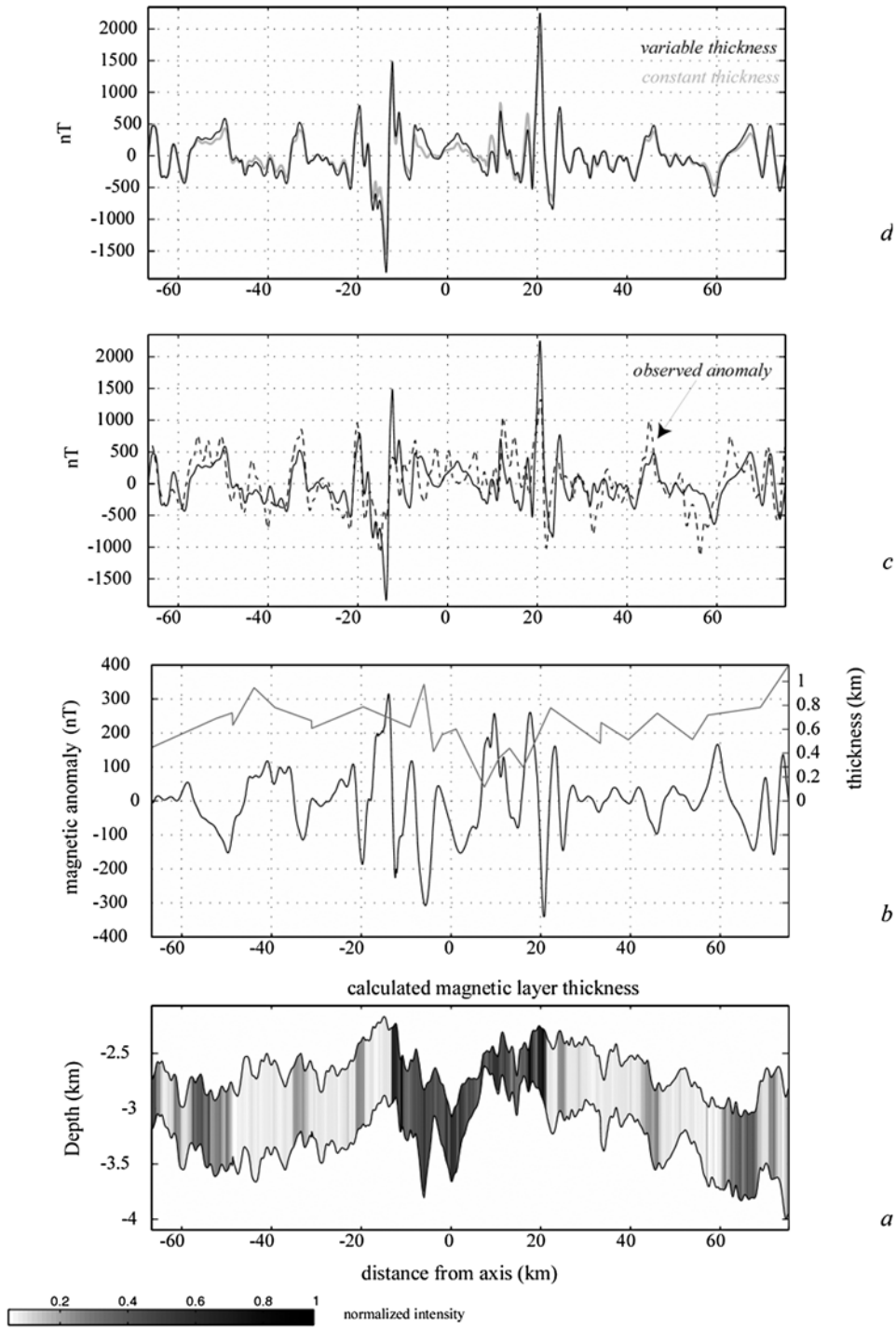

Figure 10. Observed and modeled magnetic anomalies along profile A across the Central Indian Ridge. (a) Depth of magnetic layer basement computed by wavelet method. The magnetization (20 A/m maximal value) is proportional to the relative paleofield intensities estimated by *Valet and Meynadier* [1993] (normalized VADM in A.m^2 along the profile are shown by gray scale). (b) calculated thickness. Solid line is difference between magnetic anomalies computed with constant and variable thicknesses. RMS residual between constant and variable thickness computation is 73 nT. (c) Dashed line is observed signal upward continued to a level plane 2000 m below sea level (as by *Pouliquen et al.* [2001]); data are not reduced to the pole. Solid line is model computed with observed topography, computed magnetic layer basement depth and variable magnetization. (d) Magnetic anomalies computed with constant (500 m; gray line) and estimated magnetic thickness (solid line).

in the uppermost oceanic crust carry the strongest magnetization. Such a model does not necessarily require that the top and bottom layer correspond to two distinct units (e.g., a basaltic layer on the top and an intrusive dike section below) but could involve a gradational increase of the magnetization through the pillow basalts with depth. Basalt magnetization data from DSDP Hole 504B do not show evidence for such a gradational increase, but show a considerable scatter around an average value of ~5.2 A/m, with a range of magnetizations at least 10–50 times greater than the one we considered in our model [*Smith and Banerjee*, 1986; *Pariso and Johnson*, 1991]. Given the low core recovery at Hole 504B, it is possible that the average magnetization of cored samples is not, in fact, representative of the actual drilled formations. On the other hand, the two-layer magnetic source model could be consistent with the secondary mineralogy observed on Hole 504B [*Alt et al.*, 1986], suggesting that the upper 300 m of pillow basalts have undergone low-temperature oxidative alteration. Low-temperature alteration is known to decrease the magnetization of ocean floor basalts [e.g., *Bleil and Petersen*, 1983].

[52] Whatever the geological interpretation, our preferred hypothesis is that the discrepancies between the magnetic layer thicknesses calculated at JDF with the two inversion techniques reflect distinct responses of the two techniques to source characteristics that are not taken into account in both techniques, for example, the existence of pronounced vertical heterogeneities of the magnetization.

6. Conclusion

[53] Applying wavelet transform to high-resolution marine magnetic profiles, we can constrain the location and intensity of horizontal magnetization contrasts and the thickness of the oceanic crustal magnetic layer. We achieve this by adapting a continuous wavelet-based method designed as a multipole decomposition that consists in interpreting data in the domain of their upward continued analytic signals. This method can be used as a fast interpretation technique and can be applied to raw magnetic deep-tow data. This is an advantage with regard to more classical inversion techniques which often need preprocessing (e.g., azimuth corrections of profiles, vertical continuation to correct for variations in the altitude of the deep-tow, and reduction to the pole) that can introduce artifacts in the data. The wavelet technique gives a new insight for studying the interplay between magnetization intensity and thickness of the magnetic layers within observed magnetic anomalies. This approach is particularly indicated when considering magnetic anomalies for paleomagnetic studies.

[54] This new method can be applied to any deep-tow magnetic profile but is limited, in the actual form, by a number assumptions:

[55] 1. The modeled magnetization layer has a constant magnetization along the vertical axis; horizontal variations in magnetization occur across vertical contacts that limit rectangular magnetization blocks. The method computes magnetic layer thicknesses at these model vertical contacts. Further developments of the technique to constrain the dip of contacts between magnetized blocks and the inclination of magnetization in the source are, however, possible, using the phase of complex wavelet coefficients [see *Sailhac et al.*, 2000].

[56] 2. Applied to deep-tow data, the method is best suited to handle either deep magnetic sources (> 500 m) or sources with wide-spaced magnetizations and/or thickness variations. By contrast, it is poorly fitted to analyze the source of short-wavelength anomalies (<~4–5 km).

[57] 3. The variable distance between the deep tow and the sea bottom is taken into account in the final steps of the calculation of magnetic layer thickness values, but the upward continuation procedure used in the wavelet transform assumes that the data are located on a horizontal line. The method is therefore not well adapted for the processing of profiles acquired at highly variable deep-tow altitudes (i.e., with altitude gradients >~30°).

[58] 4. The method relies on the 2-D approximation, with magnetization blocks supposed to be infinite in the horizontal direction perpendicular to profiles. This method is therefore not adapted for blocks with ratio of across profile width to along profile length, or to thickness <~3.

[59] The application of this wavelet-based technique to deep-tow magnetic profiles across both the CIR and the JDF suggests that the magnetic layer is ~600 m thick on average, and varies in magnetization and thickness (from 100 to 1200 m) over short distances (i.e., timescales). We interpret the short-scale variations of source thickness calculated with the wavelet method as due to variations of the thickness of lava flows caused either by preexisting topography or by faulting. Forward modeling confirms that the CIR upper crustal magnetic source does carry a coherent record of the past short-term geomagnetic field intensity variations. Forward modeling also suggests that variations of the magnetic layer thickness have a significant effect on magnetic anomalies when they are strong enough, or coupled to important intensity contrasts. Although information on the thickness variations can be used to improve magnetization models, our results also suggest that variations of the magnetic layer thickness across the CIR are not the first-order cause of the short to medium timescale (0.05–0.2 Myr) anomalies recorded in the deep tow profiles.

[60] **Acknowledgments.** We thank M. Tivey, who kindly provided the JDF data and helped us with fruitful discussions during the writing of the manuscript. We also thank M. Cannat for her review of early versions of this paper and D. Gibert and an anonymous reviewer for their critical reading of the submitted manuscript and their helpful advices. This is IPGP contribution 1864 and EOST/IPGS contribution 2002.25-UMR7516.

References

Allerton, S., J. Escartin, and R. Searle, Extremely asymmetric magmatic accretion of oceanic crust at the ends of slow-spreading ridge segments, *Geology*, *28*, 179–182, 2000.

Alt, J. C., J. Honnorez, C. Laverne, and R. Emmermann, Hydrothermal alteration of the 1 km section through the upper oceanic crust, deep sea drilling project Hole 504B: Mineralogy, chemistry and evolution of sea water basalt interaction, *J. Geophys. Res.*, *91*, 10,309–10,335, 1986.

Arkani-Hamed, J., Thermoviscous remanent magnetization of oceanic lithosphere inferred from its thermal evolution, *J. Geophys. Res.*, *94*, 17,421–17,436, 1989.

Babcock, J. M., A. J. Harding, G. M. Kent, and J. A. Orcutt, An examination of along-axis variation of magma chamber width and crustal structure on the East Pacific Rise between 13°30′N and 12°20′N, *J. Geophys. Res.*, *103*, 30,451–30,467, 1998.

Bina, M. M., Magnetic properties of basalts from ODP Hole B on the Mid-Atlantic Ridge near 23°N, *Proc. Ocean Drill. Program Sci. Results*, *65*, 297–302, 1990.

Blakely, R. J., Statistical averaging of marine magnetic anomalies and the aging of oceanic crust, *J. Geophys. Res.*, *88*, 2289–2296, 1983.

Blakely, R. J., *Potential Theory in Gravity and Magnetic Applications*, 441 pp., Cambridge Univ. Press., New York, 1996.

Bleil, U., and N. Petersen, Variations in magnetization intensity and low-temperature titanomagnetite oxidation of ocean floor basalts, *Nature*, *301*, 384–387, 1983.

Bott, M. H. P., Solution of the linear inverse problem in magnetic interpretation with application to oceanic magnetic anomalies, *Geophys. J. R. Astron. Soc.*, *13*, 313–323, 1967.

Canales, J. P., R. S. Detrick, J. Lin, and J. A. Collins, Crustal and upper mantle seismic structure beneath the rift montains and across a nontransform offset at the Mid-Atlantic Ridge (35°N), *J. Geophys. Res.*, *105*, 2699–2719, 2000.

Cande, S. C., and D. V. Kent, Ultrahigh resolution marine magnetic anomaly profiles: A record of continuous paleointensity variations, *J. Geophys. Res.*, *97*, 15,075–15,083, 1992.

Cannat, M., Emplacement of mantle rocks in the seafloor at mid-ocean ridges, *J. Geophys. Res.*, *98*, 4163–4172, 1993.

Carbotte, S., and K. MacDonald, East Pacific rise 8°–10°30′N: Evolution of ridge segments and discontinuities from SeaMARC II and three-dimensional magnetic studies, *J. Geophys. Res.*, *97*, 6959–6982, 1992.

Christeson, G. L., G. M. Kent, G. M. Purdy, and R. S. Detrick, Extrusive thickness variability at the East Pacific Rise, 9°–10°N: Constraints from seismic techniques, *J. Geophys. Res.*, *101*(B2), 2859–2873, 1996.

Conder, J. A., D. S. Scheirer, and D. W. Forsyth, Seafloor spreading on the Amsterdam-St. Paul hotspot plateau, *J. Geophys. Res.*, *105*, 8263–8277, 2000.

Courtillot, V., A. Galdeano, and J.-L. Le Mouël, Propagation of an accreting plate boundary: A discussion of new aeromagnetic data in the Gulf of Tadjurah and southern Afar, *Earth Planet. Sci. Lett.*, *47*, 144–160, 1980.

Detrick, R. S., A. J. Harding, D. V. Kent, J. A. Orcutt, J. C. Mutter, and P. Buhl, Seismic structure of the southern East Pacific Rise, *Science*, *259*, 499–503, 1993.

Dunlop, D. J., and M. Prévot, Magnetic properties and opaque mineralogy of drilled submarine intrusive rocks, *Geophys. J.R. Astron. Soc.*, *69*, 763–802, 1982.

Dyment, J., J. Arkani-hamed, and A. Ghods, Contribution of serpentinized ultramafics to marine magnetic anomalies at slow and intermediate spreading centres: Insights from the shape of the anomalies, *Geophys. J. Int.*, *129*, 691–701, 1997.

Dyment, J., et al., The Magofond 2 cruise: A surface and deep-tow survey on the past and present CIR, *InterRidge News*, *8*(1), 25–31, 1999.

Gee, J., and D. V. Kent, Variations in layer 2A thickness and the origin of the central anomaly magnetic high, *Geophys. Res. Lett.*, *21*, 297–300, 1994.

Gee, J., S. C. Cande, J. A. Hildebrand, K. Donnelly, and R. L. Parker, Geomagnetic intensity variations over the past 780 kyr obtained from near-seafloor magnetic anomalies, *Nature*, *408*, 827–832, 2000.

Gente, P., R. A. Pockalny, C. Durand, C. Deplus, M. Maia, G. Ceuleneer, C. Mével, M. Cannat, and C. Laverne, Characteristics and evolution of the segmentation of the Mid-Atlantic Ridge between 20°N and 24°N during the last 10 million years, *Earth Planet. Sci. Lett.*, *129*, 55–71, 1995.

Gibert, D., and A. Galdeano, A computer program to perform transformations of gravimetric and aeromagnetic surveys, *Comput. Geosci.*, *11*, 553–588, 1985.

Hansen, R. O., and M. Simmonds, Multiple-source Werner deconvolution, *Geophysics*, *58*, 1792–1800, 1993.

Head, J. W. I., L. Wilson, and D. K. Smith, Mid-ocean eruptive vent morphology and substructure: Evidence for dike widths, eruption rates, and evolution of eruptions and axial volcanic ridges, *J. Geophys. Res.*, *101*, 28,265–28,280, 1996.

Hooft, E. E. E., H. Schouten, and R. S. Detrick, Constraining crustal emplacement processes from the variation in seismic layer 2A thickness at the East Pacific Rise, *Earth Planet. Sci. Lett.*, *142*, 289–309, 1996.

Hussenoeder, S., M. A. Tivey, H. Schouten, and R. C. Searle, Near-bottom magnetic survey of the Mid-Atlantic Ridge axis, 24°–24°40′N: Implications for crustal accretion at slow spreading ridges, *J. Geophys. Res.*, *101*, 22,051–22,069, 1996.

Johnson, H. P., and T. Atwater, Magnetic study of basalts from the Mid-Atlantic Ridge, lat 37°N, *Geol. Soc. Am. Bull.*, *88*, 637–647, 1977.

Karson, J. A., et al., Along-axis variations in seafloor spreading in the MARK area, *Nature*, *328*, 681–685, 1987.

Klitgord, K. D., S. P. Huestis, J. D. Mudie, and R. L. Parker, An analysis of near-bottom magnetic anomalies: Sea-floor spreading and the magnetized layer, *Geophys. J.R. Astron. Soc.*, *43*, 387–424, 1975.

Kok, Y., and L. Tauxe, A relative paleointensity stack from Ontong-Java Plateau sediments for the Matuyama, *J. Geophys. Res.*, *104*, 25,401–25,413, 1999.

Lagabrielle, Y., D. Bideau, M. Cannat, J. A. Karson, and C. Mével, Ultramafic-mafic plutonic rocks suites exposed along the Mid-Atlantic Ridge (10°N–30°N), Symmetrical-asymmetrical distribution and implications for seafloor spreading processes, in *Faulting and Magmatism at Mid-Ocean Ridges*, *Geophys. Monogr. Ser.*, vol. 106, edited by W. R. Buck et al., pp. 153–176, AGU, Washington, D. C., 1998.

Lee, S.-M., and R. C. Searle, Crustal magnetization of the Reykjanes ridge and implications for its along-axis variability and the formation of axial volcanic ridges, *J. Geophys. Res.*, *105*, 5907–5930, 2000.

Lee, S.-M., S. C. Solomon, and M. A. Tivey, Fine-scale crustal magnetization variations and segmentation of the East Pacific Rise, 9°10′–9°50′N, *J. Geophys. Res.*, *101*, 22,033–22,050, 1996.

Macdonald, K. C., Near-bottom magnetic anomalies, assymmetic spreading, oblique spreading, and tectonics of the Mid-Atlantic ridge near lat 37°N, *Geol. Soc. Am. Bull.*, *88*, 541–555, 1977.

Macdonald, K. C., R. Hamon, and A. Shor, A 220 km^2 recently erupted lava field on the East Pacific Rise near lat 8°S, *Geology*, *17*, 212–216, 1989.

Martelet, G., P. Sailhac, F. Moreau, and M. Diament, Characterization of geological boundaries using 1-D wavelet transform on gravity data; theory and application to the Himalayas, *Geophysics*, *66*, 1116–1129, 2001.

Moreau, F., D. Gibert, M. Holschneider, and G. Saracco, Identification of sources of potential fields with the continuous wavelet transform: Basic theory, *J. Geophys. Res.*, *104*, 5003–5013, 1999.

Nabighian, N. N., The analytic signal of two-dimensional magnetic bodies with polygonal cross-section: Its properties and use for automated interpretation, *Geophysics*, *37*, 507–517, 1972.

Nabighian, N. N., Additional comments on the analytic signal of two-dimensional magnetic bodies with polygonal cross-section, *Geophysics*, *39*, 85–92, 1974.

Nazarova, K. A., Serpentinized peridotites as a possible source for oceanic magnetic anomalies, *Mar. Geophys. Res.*, *16*, 455–462, 1994.

Oufi, O., M. Cannat, and H. Horen, Magnetic properties of variably serpentinized abyssal peridotites, *Eos Trans. AGU*, *80*(46), Fall Meet. Suppl., F915, 1999.

Pariso, J. E., and H. P. Johnson, Alteration processes at Deep Sea Drilling Project/Ocean Drilling Program Hole 504B at the Costa Rica Rift: Implications for magnetization of oceanic crust, *J. Geophys. Res.*, *96*, 11,703–11,722, 1991.

Pariso, J. E., and H. P. Johnson, Do lower crustal rocks record reversals of the Earth's magnetic field? Magnetic petrology of oceanic gabbros at Ocean Drilling Program Hole 735B, *J. Geophys. Res.*, *98*, 16,013–16,032, 1993a.

Pariso, J. E., and H. P. Johnson, Do layer 3 rocks make a significant contribution to marine magnetic anomalies? In situ magnetization of gabbros at Ocean Drilling Program Hole 735B, *J. Geophys. Res.*, *98*, 16,033–16,052, 1993b.

Pariso, J. E., C. Rommevaux, and J.-C. Sempéré, Three-dimensional inversion of marine magnetic anomalies: implications for crustal accretion along the Mid-Atlantic Ridge (28°–31°30′N), *Mar. Geophys. Res.*, *18*(1), 85–101, 1996.

Parker, R. L., The rapid calculation of potential anomalies, *Geophys. J.R. Astron. Soc.*, *31*, 447–455, 1973.

Parker, R. L., and S. P. Huestis, The inversion of magnetic anomalies in the presence of topography, *J. Geophys. Res.*, *79*, 1587–1593, 1974.

Perram, L. J., K. C. Macdonald, and S. P. Miller, Deep tow magnetics near 20°S on the East Pacific Rise: A study of short-wavelength anomalies at a very fast spreading center, *Mar. Geophys. Res.*, *12*, 235–245, 1990.

Pockalny, R. A., A. Smith, and P. Gente, Spatial and temporal variability of crustal magnetization of a slowly spreading ridge: Mid-Atlantic Ridge (20°–24°N), *Mar. Geophys. Res.*, *17*, 301–320, 1995.

Pouliquen, G., Y. Gallet, J. Dyment, and C. Tamura, A geomagnetic record over the last 3 million years from deep-tow magnetic anomaly profiles across the central Indian Ridge, *J. Geophys. Res.*, *106*, 10,941–10,960, 2001.

Sailhac, P., Analyse multiéchelle et inversion de données géophysiques en Guyane française, Inst. de Phys. du Globe, Paris, 1999.

Sailhac, P., A. Galdeano, D. Gibert, F. Moreau, and C. Delor, Identification of sources of potential fields with the continuous wavelet transform: Complex wavelets and application to aeromagnetic profiles in French Guiana, *J. Geophys. Res.*, *105*, 19,455–19,476, 2000.

Schouten, H., M. A. Tivey, D. Fornari, and J. R. Cochran, Central anomaly magnetization high: Constraints on the volcanic construction and architecture of seismic layer 2A at a fast-spreading mid-ocean ridge, the EPR at 9°30′–50′N, *Earth Planet. Sci. Lett.*, *169*, 37–50, 1999.

Seama, N., and N. Isesaki, Thickness of the marine magnetic source layer obtained from vector geomagnetic field data, *Eos Trans. AGU*, *72*(44), Fall Meet. Suppl., 448, 1991.

Sempéré, J.-C., High magnetization zones near spreading center discontinuities, *Earth Planet. Sci. Lett.*, *107*, 389–405, 1991.

Sempéré, J.-C., G. M. Purdy, and H. Schouten, Segmentation of the Mid-Atlantic Ridge between 24°N and 30°40′N, *Nature*, *334*, 427–431, 1990.

Shah, A., M. H. Cormier, W. Ryan, W. Jin, A. Bradley, and D. Yoerger, High Resolution 3-D map of the Earth's magnetic field at the EPR reveals shallow dike outcrops and large-scale void space in intrusive layers, *Eos Trans. AGU*, *80*(46), Fall Meet. Suppl., F1074, 1999.

Smith, G. M., and S. K. Banerjee, Magnetic structure of the upper kilometer of the marine crust at the Deep Sea Drilling Project Hole 504B, eastern Pacific Ocean, *J. Geophys. Res.*, *91*, 10,337–10,354, 1986.

Smith, D. K., M. A. Tivey, H. Schouten, and J. R. Cann, Locating the spreading axis along 80 km of the Mid-Atlantic Ridge south of the Atlantis Transform, *J. Geophys. Res.*, *104*, 7599–7612, 1999.

Talwani, M., C. C. Windisch, and M. G. Langseth, Reykjanes ridge crest: A detailed geophysical study, *J. Geophys. Res.*, *76*, 473–517, 1971.

Tanner, J. G., An automated method of gravity interpretation, *Geophys. J. R. Astron. Soc.*, *13*, 339–347, 1967.

Thompson, D. T., EULDPH: A new technique for making computer-assited depth estimates from magnetic data, *Geophysics*, *47*, 7–31, 1982.

Tivey, M. A., Vertical magnetic structure of ocean crust determined from near-bottom magnetic field measurements, *J. Geophys. Res.*, *101*, 20,275–20,296, 1996.

Tivey, M. A., and H. P. Johnson, The crustal anomaly magnetic high: Implications for ocean crust construction and evolution, *J. Geophys. Res.*, *92*, 12,685–12,694, 1987.

Tivey, M. A., and H. P. Johnson, Variations in oceanic crustal structure and implications for the fine-scale magnetic anomaly signal, *Geophys. Res. Lett.*, *20*, 1879–1882, 1993.

Tivey, M. A., and B. E. Tucholke, Magnetization of 0–29 Ma ocean crust on the Mid-Atlantic Ridge, 25°30' to 27°10'N, *J. Geophys. Res.*, *103*, 17,807–17,826, 1998.

Valet, J. P., and L. Meynadier, Geomagnetic field intensity and reversals during the past four million years, *Nature*, *366*, 234–238, 1993.

Verosub, K. L., and E. M. Moores, Tectonic rotations in extensional regimes and their paleomagnetic consequences for oceanic basalts, *J. Geophys. Res.*, *86*, 6335–6349, 1981.

Weiland, C. M., K. C. Macdonald, and N. R. Grindlay, Ridge segmentation and the magnetic structure of the southern Mid-Atlantic Ridge 26°S and 31°–35°S: Implications for magmatic processes at slow spreading centers, *J. Geophys. Res.*, *101*, 8055–8073, 1996.

White, D. J., and R. M. Clowes, Shallow crustal structure baneath the Juan de Fuca Ridge from 2-D seismic refraction tomography, *Geophys. J. Int.*, *100*, 349–367, 1990.

White, R. S., D. McKenzie, and K. O'Nions, Oceanic Crustal Thickness From Seismic Measurements and Rare Earth Element Inversions., *J. Geophys. Res.*, *97*, 19,683–19,715, 1992.

Wittpenn, N. A., C. G. A. Harrison, and D. W. Handschumacher, Crustal magnetization in the South Atlantic from inversion of magnetic anomalies, *J. Geophys. Res.*, *94*, 15,463–15,480, 1989.

Wooldridge, A. L., C. G. A. Harrison, M. A. Tivey, P. A. Rona, and H. Schouten, Magnetic modeling near selected areas of hydrothermal activity on the Mid-Atlantic and Gorda Ridges, *J. Geophys. Res.*, *97*, 10,911–10,926, 1992.

Worm, H. U., and W. Bosum, Implications for the sources of marine magnetic anomalies derived from magnetic logging in Holes 504B and 896A, *Proc. Ocean Drill. Program Sci. Results*, *148*, 331–338, 1996.

G. Pouliquen, Total, E&P, Potential Field Methods, F-92078 Paris, France. (gaud.pouliquen@total.com)

P. Sailhac, Laboratoire de Proche Surface, EOST, 5 rue René Descartes, 67084 Strasbourg Cedex, France.